ELECTRONIC CHARACTERISTICS OF RARE EARTH DOPED GaN

SCHOTTKY DIODES

THESIS

Aaron B. Blanning, Major, USA

AFIT-ENP-13-M-03

DEPARTMENT OF THE AIR FORCE
AIR UNIVERSITY

AIR FORCE INSTITUTE OF TECHNOLOGY

Wright-Patterson Air Force Base, Ohio

Electronic Characteristics of Rare Earth Doped GaN Schottky Diodes

THESIS

Presented to the Faculty

Department of Engineering Physics

Graduate School of Engineering and Management

Air Force Institute of Technology

Air University

Air Education and Training Command

In Partial Fulfillment of the Requirements for the

Degree of Master of Science in Nuclear Engineering

Aaron B. Blanning, BS

Major, USA

January 2013

ELECTRONIC CHARACTERISTICS OF RARE EARTH DOPED GAN SCHOTTKY DIODES

Aaron B. Blanning, BS
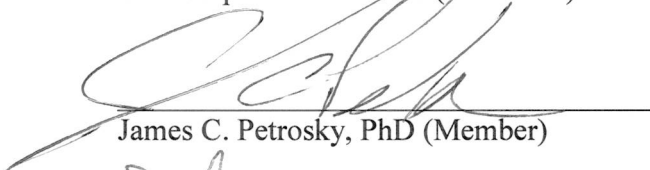Major, USA

Approved:

_____
LTC Stephen R. McHale (Chairman)
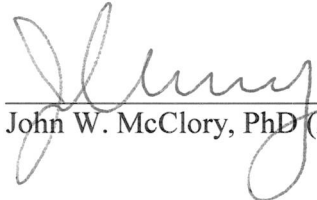
11 MAR 2013
Date

_____
James C. Petrosky, PhD (Member)

11 Mar 13
Date

_____
John W. McClory, PhD (Member)

4 MAR 2013
Date

Abstract

The Schottky barrier height (SBH) was measured on GaN based diodes with three different dopant types; gadolinium, erbium and ytterbium. Two methods were used to determine the SBH. The first method used the Jürgen Werner method to evaluate the *I-V* characteristics. This method was necessary due to the poor ideality factor of the diodes, where ideality n= 5.972, 10.311 and 10.304 for Gd-, Er- and Yb-doped diodes respectively. The calculated SBH of the diodes using the Jürgen Werner method was 1.41±0.20eV, 1.71±0.25eV and 1.75±0.28eV for the Gd-, Er- and Yb-doped diodes respectively. Larger than desired statistical error arose in these results due to error propagation in this method. An ad-hoc effective Richardson constant value of $0.006 A \times cm^{-2} \times K^{-2}$ was used to calculate the SBH, which rendered results with no greater than 2% disagreement (neglecting error) with photoemission spectroscopy measurements previously performed on the same GaN thin films by a another researcher. The second method of measuring the SBH was the temperature dependent *I-V-T* measurements using the modified Norde function. The calculated SBH of the diodes were universally lower than the results of the Jürgen Werner method. The SBH was 1.19±0.12eV, 1.39±0.16eV and 1.43±0.12eV for the Gd-, Er- and Yb-doped diodes respectively. Additionally, the Norde method provided direct calculation of the effective Richardson constants, which were $0.011±0.001 A \times cm^{-2} \times K^{-2}$, $0.036±0.003 A \times cm^{-2} \times K^{-2}$ and $0.021±0.02 A \times cm^{-2} \times K^{-2}$ for the Gd-, Er- and Yb-doped diodes respectively. Both measurements in this study are in agreement with the earlier photoemission spectroscopy measurements with regard to the

proportional differences among the different dopant types. The Yb-doped diode

exhibited the highest SBH followed by the Er and then Gd.

To my wife and our three wonderful children she has raised in my absence.

Table of Contents

List of Figures

xi

List of Tables

List of Equations

ELECTRONIC CHARACTERISTICS OF RARE EARTH

DOPED GAN SCHOTTKY DIODES

I. Introduction

1.1 General Issue

The detonation of the first nuclear weapon in 1945 created a new focus in the

advancement of radiation detection technology. Prior to the advent of nuclear weapons,

the radiation detection industry primarily concerned itself with detectors used by

academics and researchers. However, a need to detect special nuclear materials (SNM,

materials required to produce nuclear weapons) used in nuclear weapons was born from

this revelation of the destructive potential of such weapons. In the decades that followed

the Trinity nuclear weapon test, the need for new detection capabilities increased

commensurate to an ever-changing political and strategic landscape. Nation-states

developed their nuclear weapons programs and the cold war ensued, enrichment

techniques improved, and ultimately non-state (or terrorist) organizations demonstrated

aspirations to use nuclear weapons. Concerns regarding national defense and public

safety spurned a need for new detection capabilities—those aimed at detecting the unique

radiological characteristics of SNM.

Special nuclear material is defined by the NRC as ^{239}Pu, ^{233}U, ^{235}U or uranium

enriched in the isotopes ^{233}U or ^{235}U—all of which are radioactive [1]. Detectors of

SNM, for all intents and purposes, leverage the same laws of nuclear physics as any other

conventional radiation detector. One might even argue that all radiation detectors are the

same at their most fundamental level regardless of whether or not the detector is designed

1

to detect SNM or any other radioactive source. That is to say that the detector senses the radiation (such as alpha, beta, gamma, x-ray, neutron etc.) emitted from the source by presenting a material that will respond in some measureable manner due to interaction with the radiation [2]. The rest of the components in the detector serve to measure the response of the material, not the radiation itself, and convert it into a meaningful signal for the operator of the detector. Sadly, no material exists that responds uniquely to all forms of radiation at all energies, which accounts for the vast array of radiation detectors currently available—each sensitive to limited types of radiation within limited energy ranges and designed for limited purposes. Detectors for SNM must be designed such that the particular radioactive characteristics of SNM fall within the detector's limitations.

For special nuclear materials, the particular radioactive characteristics of fissile uranium (^{233}U and ^{235}U) and plutonium (^{239}Pu) must fall within the limitations of the detector. These isotopes primarily undergo alpha decay [3, 4], which might compel one to say a detector for SNM must detect the alpha particles, the gamma radiation arising from the alpha decay, or both. However, this approach becomes problematic because alpha particles have a comparatively short mean free path making them easily shielded from detection [2]. Gamma rays are more penetrating than the alpha particles, but distinguishing a gamma ray emitted by SNM from a gamma ray emitted by various other gamma sources poses difficulties not easily overcome. For example, distinguishing SNM from other radioisotopes (such as some used in medicine) using a gamma radiation detector on the outside of a shipping container would be problematic and impractical. The original energies of the gamma rays would be difficult to determine due to down scattering, and without knowledge of the original energy, it is difficult to narrow down

the type of radiation source [2]. So what characteristics of SNM can a radiation detector

exploit to effectively distinguish the SNM from other radioisotopes to a reasonable

degree of certainty?

A special property of SNM that allows discernment from other radioisotopes lies

not in the primary decay mode but the fact that some fissile materials undergo

spontaneous fission [7]. If the neutrons emitted from these spontaneous fission events are

above that of background radiation, they may offer telltale evidence that the material is

fissile (i.e. potentially SNM). Some SNM isotopes, such as ^{233}U, rarely emit neutrons at

rates above background, but others, are such as ^{240}Pu, which emit at much higher rates.

Since neutrons are reasonably penetrating, it stands to reason that a neutron detector

tailored to the energy range of those produced from particular SNM fissions would

present itself as a more attractive option than an alpha or gamma radiation detector for

the purposes of detecting SNM. However, neutron detectors come with their own set of

problems.

The spontaneous fissions of ^{240}Pu produce fast neutrons carrying an energy of

about 1MeV [5]. Accordingly, an SNM radiation detector must be capable of down-

scattering these neutrons to thermal energies and using a material sensitive to thermal

neutrons. ^{3}He gas filled detectors are problematic due to the expense and rarity of ^{3}He.

Boron triflouride (BF_3) gas-filled detectors are more common, but they are fragile, and

BF_3 is toxic [2]. Gas filled detectors using chambers lined with ^{10}B offer less toxicity,

but their efficiency is nearly half of BF_3 detectors due to the reaction taking place at the

surface, resulting in only 50% of the reaction products going into the detector volume

while the other half escaping it [2]. Additionally, gas filled detectors are inherently less

efficient because the range of a neutron in a gas is orders of magnitude higher than the range of a neutron in a solid [2]. Lithium (^{6}Li) impregnated, glass scintillating fiber detectors show promise [6], but they are currently only used in stationary applications due to their large size and fragility. Evidently the field of neutron detectors has room for improvements.

One potentially promising technology might be one that uses gadolinium (^{157}Gd) because of its comparatively high thermal neutron cross-section [2]. The thermal neutron cross-section of a material corresponds to the probability of reacting with a thermal neutron [7]. This means that a thermal neutron traveling through a material with a low thermal cross-section has a high likelihood of passing through the material without interacting (and consequently, undetected), while the same neutron traveling through a material with a high thermal cross-section has a low probability of escaping without interacting. Table 1 shows the thermal neutron cross-sections of the most commonly used isotopes in neutron detection plus the cross-section of ^{157}Gd. The difference in thermal cross-section of two orders of magnitude warrants exploring the possibility of using ^{157}Gd as a material in a neutron detector.

Table 1. Thermal Neutron Cross-Sections of Various Detector Materials

Isotope	^{3}He	^{6}Li	^{10}B	^{157}Gd
Cross-section in kilobarns	5.3	0.9	3.8	253

Based on the relatively high probability of interaction, a desirable theoretical thermal neutron detector using Gd may possess qualities of compactness, sturdiness and high efficiency. A solid-state detector using a Gd-doped semiconductor may satisfy

some of these qualities, which requires a comprehensive understanding of the semiconductor. One such semiconductor is gallium nitride (GaN).

Stephen McHale of the Air Force Institute of Technology (AFIT) performed a study of three different rare earth doped GaN thin films; (doped with gadolinium (Gd), ytterbium (Yb) and erbium (Er) [7]. McHale and others [2] assert that Gd-doped GaN fails as a candidate for semiconductor in thermal neutron detectors. The reasons that Gd-doped GaN is unsuited as a semiconductor lie not in the properties of the material itself, but in the limitations of current technologies required to build a working detector. Those limitations relate to preamplifier noise, crystal lattice growth capabilities and the ability to construct a diode capable of achieving the required electric potential needed to create a sufficient depletion region within the detector. This does not mean, however, that research on Gd-doped semiconductors should be abandoned.

Development of radiation detectors emerged from the technological advancements of multiple scientific disciplines including materials science, solid-state physics, electrical engineering, and nuclear science. Naturally, one field may make advancements before the others, whereupon the findings must be put on the shelf until the other technologies can catch up, which is possibly the case with Gd-doped GaN. A holistic and in-depth understanding of this material provides the other technical disciplines a reference point, or goal, that they may aim to achieve in their own developments. For example, detector preamplifier designers can use the known characteristics of Gd-doped GaN to establish a maximum acceptable noise level in their designs.

McHale's work showed that doping GaN with the three rare earth elements listed above has meaningful impact upon the electrical characteristics of the semiconductor. Most notably, doping the GaN with Gd, Er or Yb increased the Schottky barrier height by 25-55% above that of undoped GaN [7]. He determined the Schottky barrier heights by using photoemission spectroscopy. The research presented here aims to augment McHale's work by the measuring the Schottky barrier heights of the same thin film samples using different measurement techniques, an *I-V* method and an *I-V-T* method using the Norde function.

1.2 Objective

This research is aimed at determining the Schottky barrier height, SBH, of three different rare earth doped (Gd, Er and Yb) gallium nitride (GaN) thin film samples via current-voltage (*I-V*) characterization and temperature dependent *I-V* characterization using the modified Norde function. The results of the measurements will be compared with previous photoemission spectroscopy measurements performed on the same samples [7].

The work focused on three areas.

1. Construction of Schottky diodes on the original GaN thin films: For comparison between the measurements performed in this study and McHale's photoemission spectroscopy measurements, it was paramount to use the same samples that he used. Thus, determining the appropriate design and construction method for applying Schottky contacts to the thin films lies at the heart of attaining reliable measurements.

2. *I-V* characterization of the diodes: *I-V* measurements were taken after depositing the Schottky contacts on the thin films. An appropriate mathematical method was applied to evaluate the raw data of the diodes and determine the SBH.

6

3. *I-V-T* characterization of the diodes: The modified Norde method [9] was used for measuring the SBH by incorporating temperature dependence of the *I-V* relationship.

II. Theory

2.1 Semiconductor Detector Operation

2.1.1. Overview

In the following sections, we shall consider a theoretical semiconductor neutron detector and then address obstacles in turning this theoretical concept into an actual detector. Semiconductor detectors, often referred to as solid-state detectors, offer several advantages over other types of detectors. Compared to gas filled detectors, the size of a semiconductor detector is typically significantly smaller because of the higher density of the detection medium—a difference of about 1000 times in many cases [2]. The gas filled detectors must be larger in order to accommodate the large neutron range relative to that of a semiconductor. Compared to scintillation detectors, the energy resolution of semiconductor detectors is generally superior [2]. In scintillation detectors, a radiation event in the cathode of the detector causes the emission of a relatively small amount of electrons, which then must cause a cascaded within the photomultiplier tube before being registered at the anode. The sheer number of steps that must take place in order to convert the radiation into light, and then convert again into a usable electrical signal, makes the system inherently inefficient. Another desirable feature of semiconductor detectors is that the operator of can adjust the thickness of the effective depletion region; the region where radiation events are most likely to produce a measurable signal. Additionally, semiconductors can produce far more information carriers (in this case electron-hole pairs) per single radiation event than most other common detector types [2].

2.1.2. Basic Semiconductor Properties

Semiconductors maintain a periodic arrangement in their atomic structure, referred to as a *crystal lattice* or *periodic lattice* [9, 10]. As a consequence of the crystal lattice, the electrons are confined to energy bands, or more importantly, there exist prohibited energy levels that the electrons may not occupy [9, 10, 11]. The prohibited energy levels fall within ranges forming bands known as *energy gaps* or *band gaps* [9, 10, 11]. Figure 1 shows the relative size of the band gap in different categories: insulators, semiconductors and metals (a.k.a. conductors). Also depicted in the figure are the two highest allowable bands; the *valence* and *conduction bands* [9, 10, 11]. Lower energy electrons that are strongly bound to a specific atom reside in the valence band. Electrons that are available to move from one atomic site to another exist at energies within the conduction band [11].
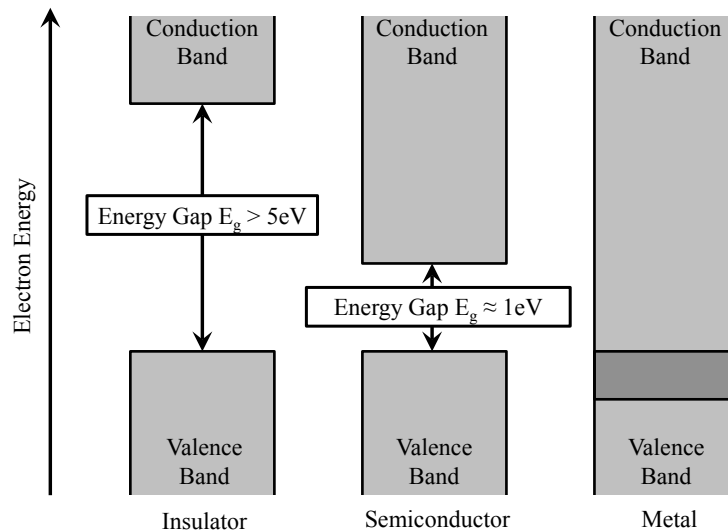
Figure 1. Energy band diagrams of insulators, semiconductors, and metals.

The size of the band gap determines the classification of the material [9]. Materials with a large band gap are classified as insulators because of the large amount of energy required to move an electron into the conduction band. Metals (a.k.a. conductors) have overlapping valence and conduction bands (or sometimes a partially filled valence band), which means there are always electrons that are able to move about the material in response to magnetic or electric fields. What makes a semiconductor so special is the relatively small band gap [10].

The relatively small band gap of semiconductors allows for controlling the amount of electrons in the conduction band and hence the current density when the semiconductor resides in an electric field. The probability of on electron occupying a given energy level is determined by Fermi-Dirac statistics. Figure 2shows that at absolute zero the electrons only occupy the energy levels up to the Fermi energy (There will be more details regarding what the Fermi energy is in the following sections). At temperatures above absolute zero, there is a probability of finding electrons occupying energy levels above the Fermi level. As temperature increases, so does the probability of electrons occupying even higher energy levels. Thus, in a semiconductor at absolute zero, all of the electrons would exist in energy states at or below the top of the valence band, committing them to individual atoms. No electrons would exist in the conduction band, and no current would flow through the material [9]. The semiconductor would behave electrically the same as an insulator under these conditions. Increasing the temperature, i.e. adding thermal energy, increases the probability that electrons will occupy energy levels at the conduction band minimum and higher. So the properties of a relatively small band gap and Fermi-Dirac statics allow us to control the number of

electrons in the conduction band by simply controlling the temperature of the

semiconductor. This is why some semiconductor radiation detectors, such as high-purity

germanium, require cooling.

Could thermal energy be applied to an insulator to get elections into the

conduction band? The answer is "technically yes", but because the band gap in an

insulator is comparatively large, the thermal energy would have to be so high that

chemical bonds would break, and in many cases the melting point of the material would

be exceeded.
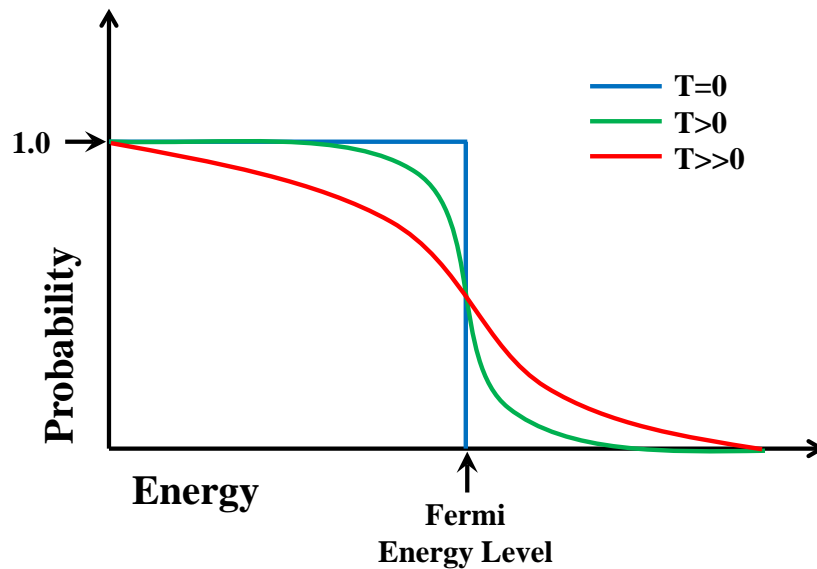
Figure 2. Fermi-Dirac probability function for electrons occupying given energy levels.

The small band gap of the semiconductor allows the application of a given

amount of energy to the material to excite some of the electrons into the conduction band

without damaging the material. The vacancies left in the valence band by the electrons

are known as *electron holes* (see Figure 3) [8,9]. The energy imparted into the material

by a radiation event (or any energy source for that matter) creates electron-hole pairs, which, when placed in an electric field, creates a measureable current if enough electron-hole pairs are created [2]. Current produced by electron-hole pairs lies at the heart of semiconductor radiation detection, and we shall exploit this as we consider our theoretical semiconductor neutron detector. But first, a better understanding of how semiconductors are used to detect ionizing radiation must be developed before addressing detection of non-ionizing radiation such as neutrons.
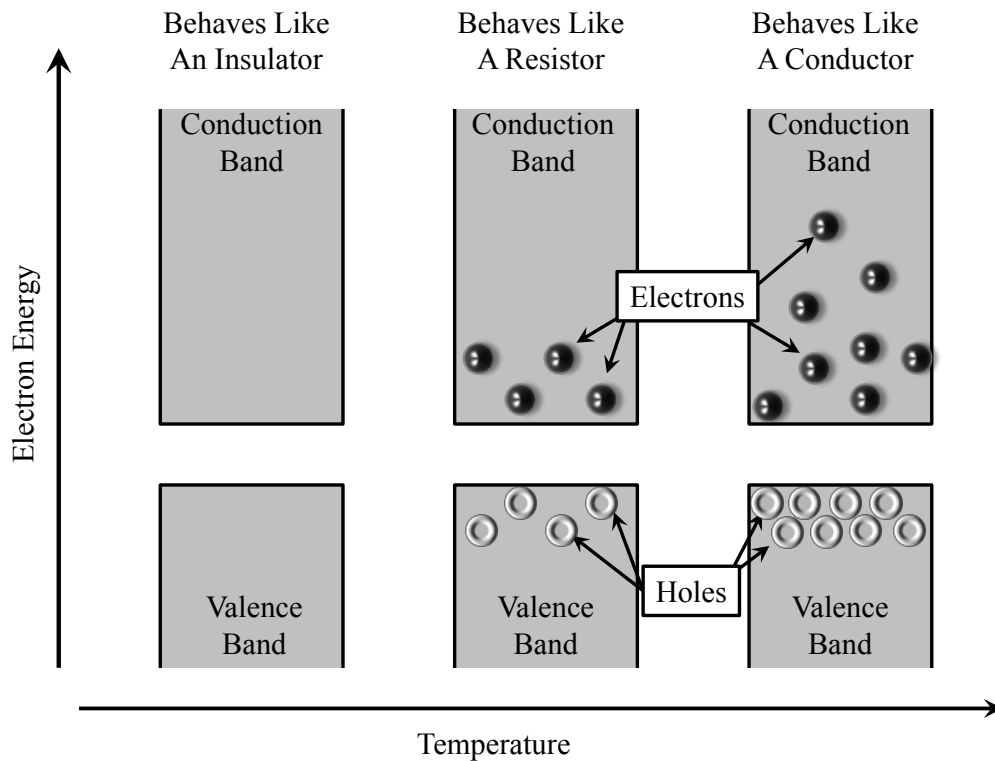
Figure 3. Filling of energy bands of a semiconductor with increasing temperature. The number of electrons available to move freely about the material increases as thermal energy is added to the system changing the electrical properties of the material.

2.1.3 Using Semiconductors as Radiation Detection Materials

The electron-hole pairs produced in a semiconductor serve as the signal carriers in radiation detection [2]. Energy greater than or equal to the band gap (the difference between the bottom of the conduction band and the top of the valence band) must be added to an electron in order to excite the electron to the conduction band, leaving behind an electron hole in the valence band. Once in the conduction band, the electron is free to move about the material, but soon after, the electron and hole can be expected to recombine [9]. If the material is in an electric field, the electron and hole will likely be swept away from each other before they have a chance to recombine [10, 11]. Given a sufficient number of electron-hole pairs, the movement of the electrons and holes in the material constitute a measureable current. This current is used as the signal in the radiation detector [2].

Figure 4 depicts our simple theoretical semiconductor radiation detector for ionizing radiation. Ionizing radiation moves through the semiconductor creating a path of electron-hole pairs via Compton scattering or the photoelectric effect. Because an electric field is applied to the semiconductor, the electrons and holes migrate away from each other mostly before recombination can occur. An ammeter registers the current produced by the movement of the electrons and holes, which constitutes a count for a single radiation event. This is a simplified explanation of a semiconductor detector, which neglects such problems that occur from impurities, dopants, trapping, recombination et cetera.
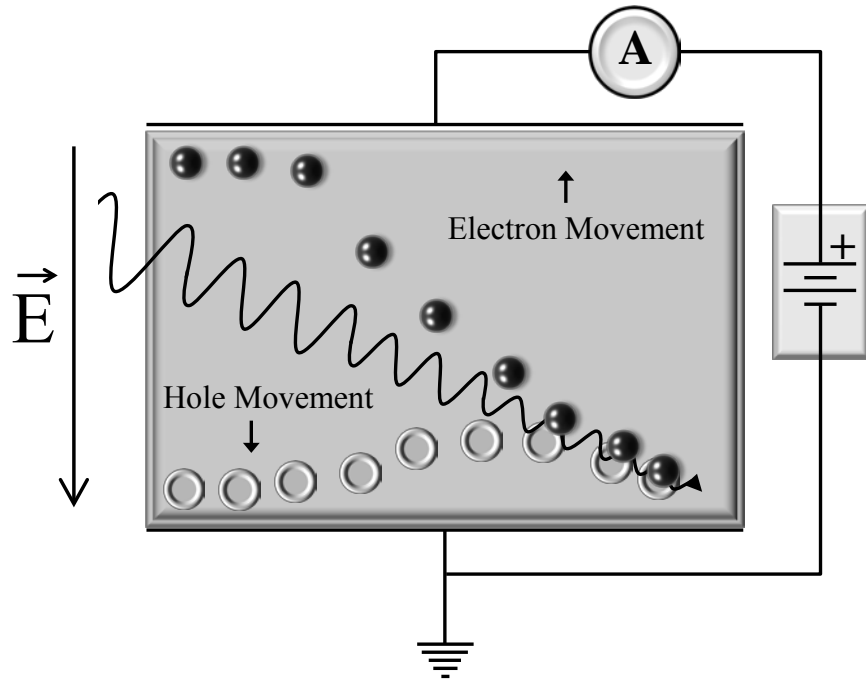
Figure 4. Diagram of a simple theoretical semiconductor radiation detector system. When ionizing radiation enters the solid state medium, it creates a path of electron-hole pairs. Because the medium is in an electric field, the electrons and holes migrate away from each other to the opposite ends of the material, which creates a measurable current.

Until this point, only ionizing radiation has been considered in the operation of a semiconductor detector. The means by which a semiconductor detector can be used to detect the type of radiation of interest in this study, neutron radiation, shall now be addressed.

In order to detect non-ionizing radiation such as neutrons, an intermediate step that responds to the neutron and subsequently produces an ionizing event must occur [2]. Gadolinium, with its high neutron capture cross section, produces two types ionizing radiation as a result of neutron capture [4] as shown in Figure 5. Initially, the neutron is captured by a gadolinium atom resulting in a compound nucleus,

14

$$\,^{157}_{64}\text{Gd} + \,^{1}_{0}\text{n} \;\rightarrow\; \,^{158}_{64}\text{Gd} * .$$
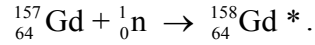
Subsequently, the ^{158}Gd product de-excites via one of several possible processes (see Figure 5). 19.1% of these processes are well documented [7] and are shown in Table 2. Ultimately, one can expect the de-excitation to result in an electron with energy of 6, 35, 72 or 174 keV, or a number of photons of energies ranging between 7 keV and 6.7 MeV. Whether the emission is in the form of an internal conversion electron or a photon, the result is ionizing radiation. The photons likely escape the material without producing enough electron-hole pairs. Due to energy and mean free path, it is the 72 keV internal conversion electron that we count on to produce enough electron-hole pair signal carriers to detection radiation in our theoretical semiconductor neutron detector.

a. Neutron is captured by the ^{157}Gd

b. The ^{158}Gd* compound nucleus is formed

or

c. The ^{158}Gd de-excites producing an Auger electron or the ^{158}Gd de-excites producing a γ-ray or X-ray.
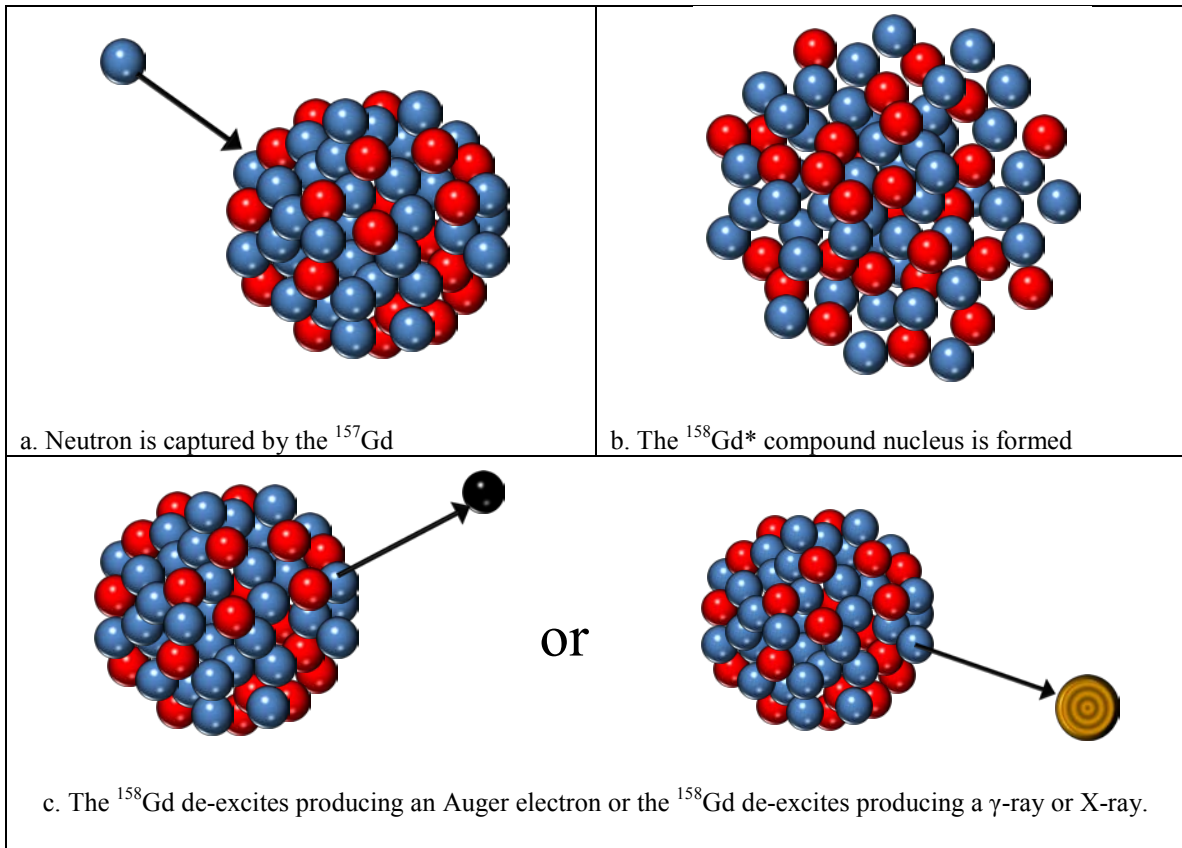
Figure 5. How ^{157}Gd converts a neutron into usable ionizing radiation. 4.a. Shows the neutron capture followed the by excited compound nucleus in 4.b. The ^{158}Gd de-excites producing either an Auger electron or a photon (4.c.)

Table 2. Ionizing radiation produced from ^{158}Gd de-excitation

Adapted from McHale [7].

Absolute Intensity	Radiation Produced	Radiation Energy
3.4%	IC Electron	72 keV
	K-shell X-ray	43 keV
	L-shell X-ray	7 keV
1.4%	IC Electron	174 keV
	K-shell X-ray	43 keV
	L-shell X-ray	7 keV
7.9%	γ-ray	79 keV
3.2%	γ-ray	182 keV
1.5%	γ-ray	1.1 or 6.7 MeV
	KLL Auger Electron	35 keV
	KMM Auger Electron	6 keV

16

A theoretical semiconductor neutron radiation detector using gadolinium might work as follows (see Figure 6). First, the neutron enters a gadolinium-doped semiconductor. Next, the neutron is captured by a gadolinium atom, and the gadolinium subsequently de-excites emitting ionizing radiation. Then, the ionizing radiation creates electron-hole pairs that serve as signal carriers in the semiconductor, which are swept apart by an electric field. Finally, the current generated by the movement of the electrons and holes is used to process the signal [2].
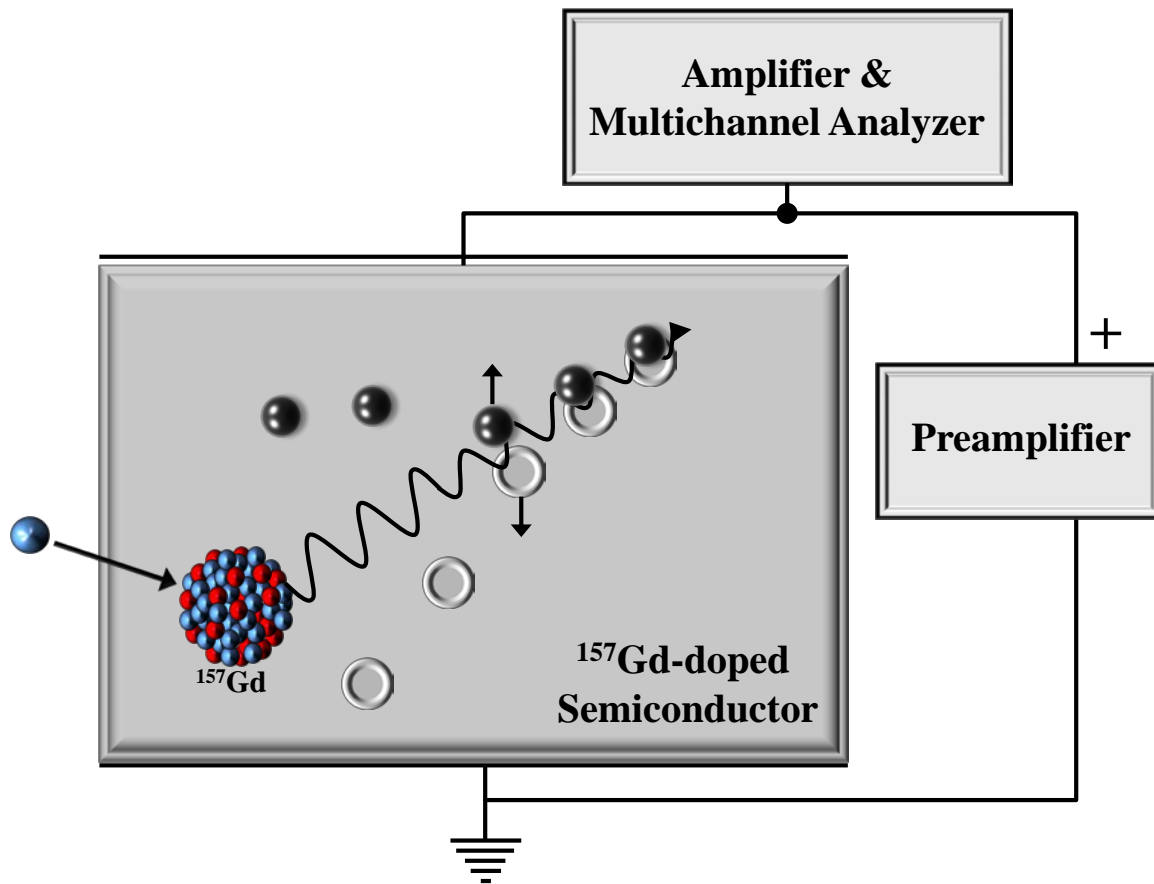
Figure 6. Theoretical Gd-doped semiconductor neutron radiation detector.

2.1.4 Coupling the Semiconductor Detector to the Electronics

The final step in building our theoretical semiconductor neutron detector is creating the electric field within the semiconductor. The challenge lies in creating an electric field without inducing current in the material from the movement of conduction band electrons and holes that exist even in the absence of radiation imparted energy. Cooling may be an option, but as discussed in previous sections, this would mitigate the benefits of small size and portability that solid state detectors might offer. Recall from section 2.1.2 that in order for all of the electrons to leave the conduction band and fall into the valence band, where they become committed to a specific atomic site, there must be a *nearly complete absence of available energy* for the electrons to use to get into the conduction band. This includes thermal energy. So at room temperature one should expect some electrons to exist in the conduction band. Consequently one would see small currents in a room temperature semiconductor in an electric field due to these thermally excited electrons in the conduction band [2, 10, 11]. As temperature increases, conductivity increases to a point, until limited by scattering from phonons within the semiconductor.

Detector designers sometimes mitigate currents from thermally excited electrons by cooling the semiconductor as close to absolute zero as possible, which removes electrons from the conduction band [2]. In most cases, moderate cooling from conventional refrigeration equipment fails to achieve a significant effect in reducing the fraction of electrons in the conduction band, so designers use alternate cooling means such as using liquid nitrogen (many high purity germanium-based detectors use this cooling method) [2]. This is especially necessary in the case of germanium-based

detectors due to the smaller band gap of germanium and hence the greater susceptibility to thermally excited electrons appearing in the conduction band. In addition to the added maintenance, using liquid nitrogen negates some of the incentives for using semiconductor detectors; such as size, weight, and portability.

Another option used by semiconductor radiation detector designers is to grow the semiconductor crystal such that it behaves like a diode. A diode is a rectifying device, that is to say it allows current to flow in one direction but effectively blocks current flowing in the opposite direction. The idea is create an energy barrier that the electrons must overcome in order to continue moving. Thus, an electron must not only have enough energy to be in the conduction band, but it must also have energy above that of the conduction band minimum sufficient to overcome the barrier. When the diode blocks current flow, it is said to be under *reverse bias* [9, 10]. The reverse bias condition preserves the electric potential we need to create the electric field but greatly reduces the current. In theory, an ideal diode would completely block the current, but this has never been achieved in practice [9, 10, 11]. In the interest of this research, two basic diode designs will be discussed; the *p-n* diode (for illustrative purposes), and the Schottky diode.

The *p-n* diode function depends on doping. Dopants are impurities in the crystal lattice of the semiconductor that alter the electrical properties of the material [9, 10, 11]. All semiconductors have some amount of dopant as a consequence of impurities that could not be removed during purification or the crystal growth process [2, 9]. However, impurities are often deliberately included in the crystal growth process to achieve a specific electrical property [9, 10]. The two types of semiconductor types that arise from

doping are *n*-type and *p*-type, which are electrically negative and positive respectively [9, 10]. Figure 7 shows an example of silicon doped with phosphorus (*n*-type). It is also possible to dope a material such as silicon with something such as boron, which has one less electron, to make it *p*-type. Doping effectively creates an imbalance of electrons vs. holes within the semiconductor. The excess electrons in the *n*-type material require comparatively little energy to excite them into the conduction band [9, 10]. This property is important in that the electron will easily diffuse in the material.
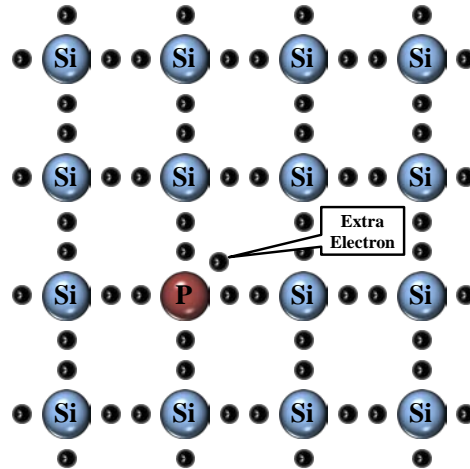
n-type silicon
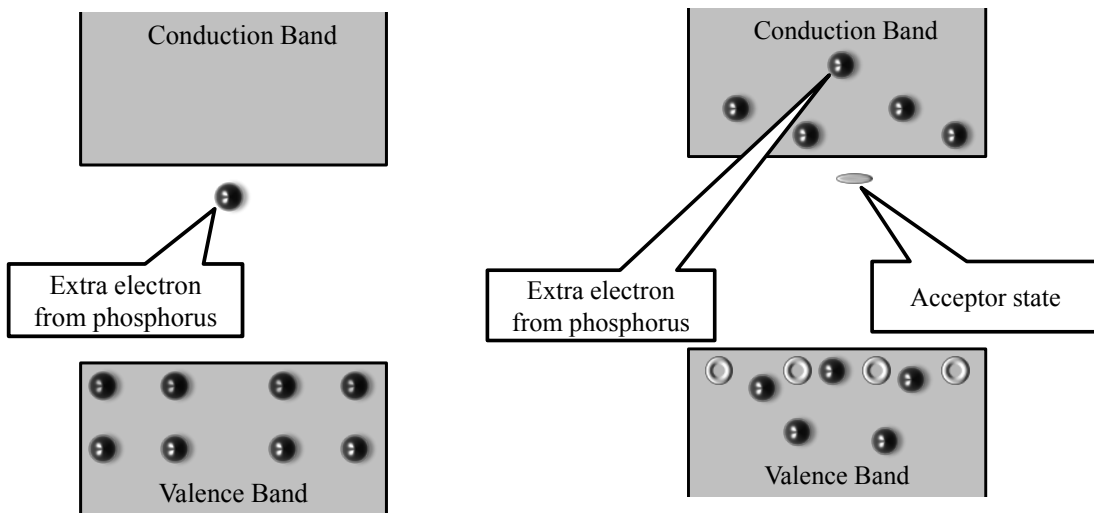
a. Exmple of *n*-type silicon at 0K   **b. Example of *n*-type silicon at room temperature**

Figure 7. Examples of *n*-type silicon. By adding an element with an extra valence electron, the electrical properties of the material becomes altered. Notice that the loosely bound extra electron in the *n*-type semiconductor requires comparatively little energy to excite into the conduction band. So at room temperature one can expect the electron to reside in the conduction band, leaving an acceptor state in the band gap.

The diode is manufactured by growing the crystal such that there are essentially

two parts, an *n*-type and a p-type. Figure 8 shows a theoretical *p-n* diode. When no bias

is applied a depletion region exists where free electrons from the *n*-type material diffuse

into the *p*-type material creating negative ions and leaving behind positive ions. Simultaneously, excess holes in the *p*-type material diffuse in the opposite direction [9]. The space charge buildup in the depletion regions creates an electric field, or *drift field* [7], in the opposite direction as the field created by the *p*- and *n*-type materials, or *diffusion field* [7]. This inhibits further electron movement across the junction [9]. Applying a forward bias overcomes the drift field in the depletion region, making the depletion region smaller (smaller than what is depicted in Figure 8.b., which is only shown for illustrative purposes), and allowing electrons and holes to migrate across the junction [10, 12]. Conversely, a reverse bias complements the drift field in the depletion region making the depletion region larger, thus further inhibiting electron and hole migration across the junction [10, 12]. However, the reverse bias condition achieves the condition of creating a larger electric field plus a larger depletion region while still minimizing undesired current [2].
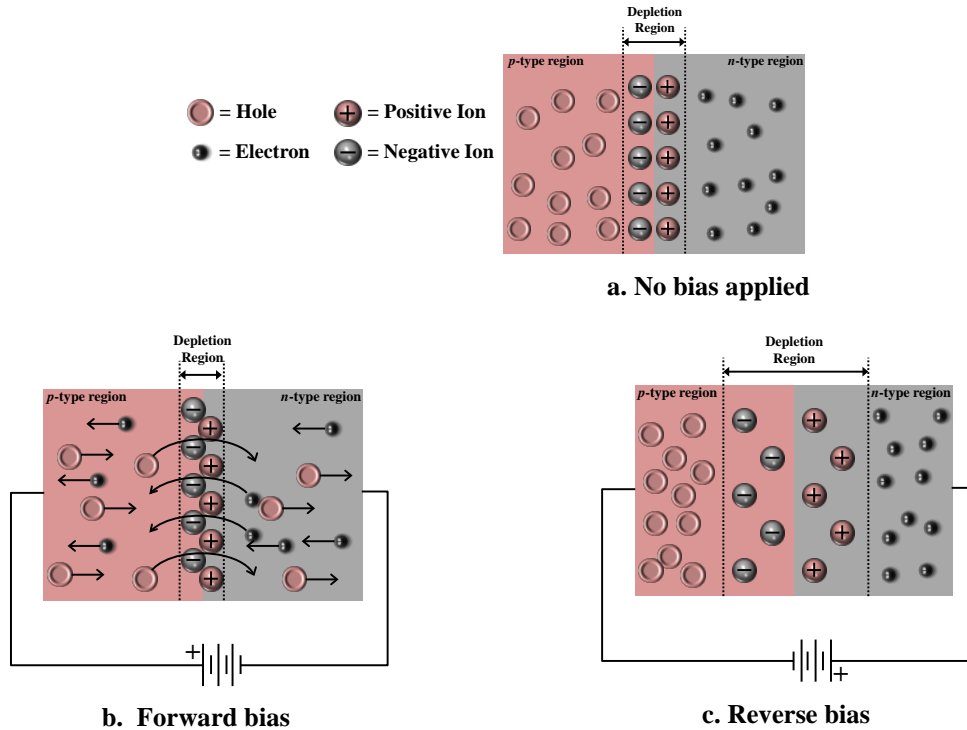
Figure 8. Diagram of a theoretical *p-n* diode. 9.a depicts a *p-n* diode with no applied bias. When a forward bias is applied (9.b.), the electric field of the depletion region is overcome, and electrons and holes are permitted to migrate. When a reverse bias is applied (9.c.) the electric field of the depletion region is augmented and the width of the region increases making it more resistive to electron and hole migration across the junction.

Finally, we have everything we need to build our theoretical semiconductor diode neutron detector (see Figure 9). The sequence of operations in the detector would occur the same as it would for the detector depicted in Figure 6 with the addition of a *p*-type region and an *n*-type region to facilitate producing an electric field that induces a current from the electron-hole production.

A detector that operates in a similar manner might also work with the use of a Schottky diode rather than a *p-n* diode [2]. The details of Schottky diode operation will be discussed in Section 2.2.
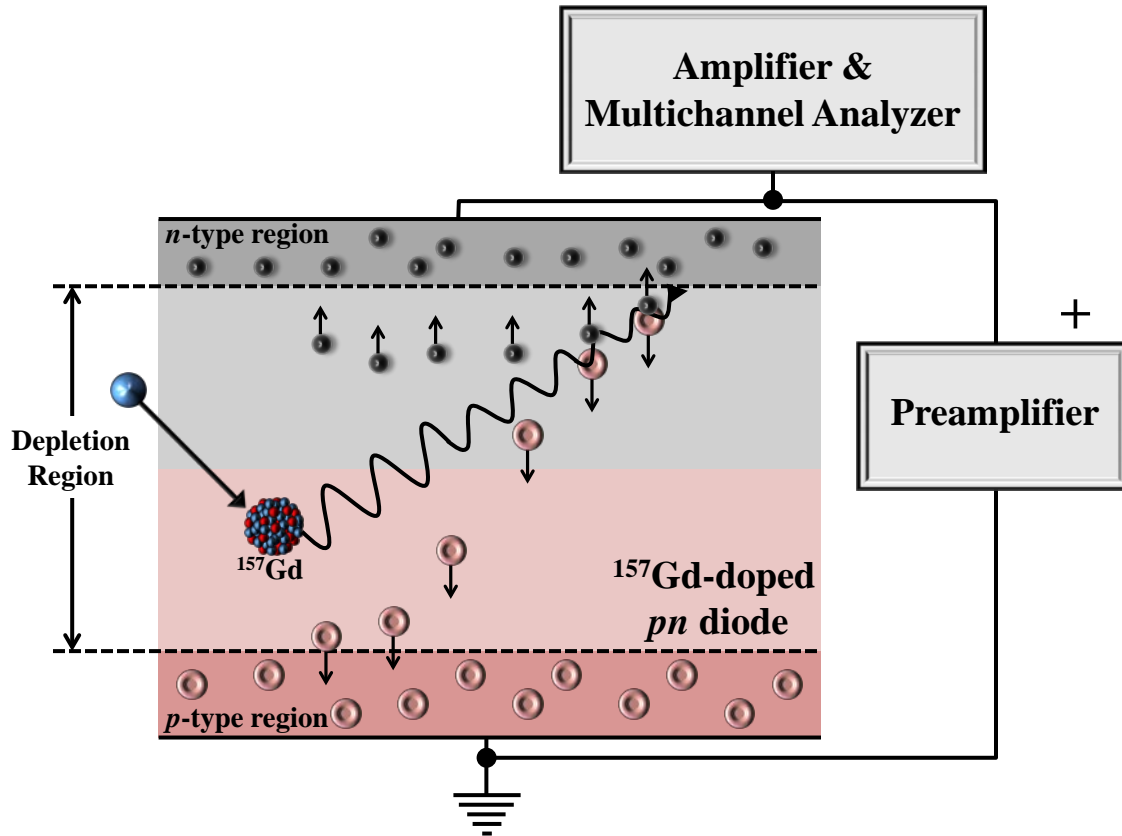
Figure 9. Theoretical semiconductor diode neutron detector.

2.1.5 Why Gadolinium Doped Detectors Won't Work in 2013

At this point, the reader may be wondering why Gd-doped semiconductor

detectors are not already in production. Previous research addressed the requirements for

the physical construction and operating conditions of a Gd-doped semiconductor neutron

detector and found it to be impracticable for three basic reasons [7]. The reasons relate to

the necessary semiconductor material thickness; the magnitude of the required bias

applied to the semiconductor diode; and the inherent preamplifier noise levels.

Semiconductor Material Thickness

The required thickness of the semiconductor material is driven by the mean free paths of the radiation events [2]. The mean free path is determined by the energy of the radiation and the nature of the material the photon or electron is passing through [3]. Thus, the material thickness of the semiconductor must be greater than the mean free path to ensure the maximum number of electron-hole pairs are produced per radiation event [2]. McHale estimates that a depletion region must have a width of at least 30-40µm in order to accommodate the full energy deposition of the 72 or 174 keV internal conversion electrons resulting from ^{157}Gd + n capture events. Naturally, the semiconductor itself must be thicker than the depletion region, and current GaN crystal lattice growth techniques makes production a bulk material this thick cost prohibitive.

Required Bias

Even if a GaN semiconductor greater than 40µm thick were achievable at a reasonable cost, we would need to be able to apply a bias sufficient to create the 30-40µm thick depletion region. The magnitude of the necessary reverse bias in such conditions would be greater than 50 V [7]. Not only does a bias requirement this great inhibit low voltage operation of the detector, it might also exceed the voltage breakdown of the diode if the size and shape of the Schottky contact and its associated electric field gradient at the edges are not accounted for. Voltage breakdown occurs when the bias applied to the diode creates an electric field strong enough to break valence band electrons from their corresponding atoms, which then are accelerated to the extent that they have enough

energy to knock other electrons out of their orbits and create an "avalanche" of electrons [10, 12]. The avalanche effect produces a significant spike in current that usually damages the crystal lattice via Joule heating and ionization [10]. Needless to say, in order to prevent voltage breakdown, an exceptionally sturdy diode must be constructed, which potentially adds to the complexity and expense of producing the device.

Preamplifier Noise

Finally, even if the challenges of the physical size of the semiconductor and the required bias are overcome, one must contend with the noise levels of the preamplifier. Current commercial preamplifiers carry a noise charge of roughly 0.1-1.2 fC [7]. The charge generated by a single radiation event is

$$Q_{\max} = \frac{E_{ion}}{3 \times E_{gap}}\left(1.6 \times 10^{-19}\right),$$ (1)

where:
$Q_{\max}$ = The maximum charge
E_{ion} = Energy of the internal conversion electron
E_{gap} = Bandgap of the semiconductor

This results in a charge generation of less than 5fC [7]. Thus the noise levels of common preamplifiers must be reduced before a Gd-base semiconductor diode detector is feasible.

McHale, however, points out, "This is not so say that development of novel solid state neutron detectors using gadolinium should be abandoned, but until the pulse processing electronics necessary to detect a neutron induced signal are improved, the

26

endeavor may prove vexing." In other words, due to technology limitations Gd-based semiconductor diode detectors cannot realistically be commercially produced........yet.

2.1.6 Another Justification For RE-Doped GaN Research

Thus far, the only justification for research on GaN doped with rare earths has been aimed at neutron detection in the SNM detection industry. And as we have previously determined, the research only serves to establish a record of the material properties for future reference assuming other technologies can catch up. Yet there exists another domain in science that may find this research relevant today—the semiconductor device and semiconductor lighting industry.

Semiconductor lighting has gained heightened interest in the lighting industry. A light emitting diode (LED) consumes a fraction of the energy per lumen than older lighting technologies including tungsten bulbs, fluorescent tubes, halogen bulbs and mercury vapor bulbs to name a few [14]. Additionally, LEDs have a far longer life expectancy than other lighting options [14]. Yet LED lighting is still a burgeoning industry, which warrants continued research and development.

Previous research suggests that GaN-based Schottky diodes exhibit an increased Schottky barrier height of 25-50% when doped with Gd, Er or Yb [7]. This is of interest in the LED industry because increasing the Schottky barrier height of a diode will decrease the leakage current of the diode; increasing its efficiency [12]. Additionally, the research suggests that the wavelength of the emitted light from GaN can be tuned to a desired length by controlling the amount of dopant within the GaN crystal lattice. In short, the electrical characteristics of rare earth doped GaN (specifically Gd-doped GaN)

may fail to garner immediate interest in the realm of SNM detection, but it may in with semiconductor devices and lighting.

2.2 Schottky Diodes

A Schottky diode performs a similar function as a *p-n* diode in that it effectively blocks current in one direction while allowing current to flow in the other direction. When used in a semiconductor diode radiation detector, a Schottky diode could be employed in the same capacity as the *p-n* diode that we used in our theoretical detector [2]. However, the construction of a Schottky diode is markedly different than a *p-n* diode. A Schottky diode is composed of a metal joined to a semiconductor, in contrast to a *p-n* diode, which is composed of a *p*-type semiconductor joined to a *n*-type semiconductor [11]. As a consequence, rectification occurs as a result of a difference in the *work functions* of the metal and the semiconductor in the Schottky diode, in contrast to the non-uniform doping profiles of the *p-n* diode [11]; the work function is the minimum amount of energy required to remove an electron from the material. So by putting metal contacts on the rare earth doped GaN thin films from McHale's work, the Schottky barrier height (SBH) of the semiconductor can be measured in a manner different than his method (photoemission spectroscopy).

2.2.1 Schottky Diode Theory of Operation

Conduction in a Schottky diode is not controlled by the recombination of minority carriers in the semiconductor as it is in a *p-n* diode [11]. A Schottky diode is a majority carrier device that leverages the thermally excited emission of the majority carriers over

28

the barrier created by the difference in work function between the metal and the

semiconductor [10]. In the case of n-type semiconductors, the majority carriers would be

electrons. For convenience, the semiconductor material shall be assumed to be n-type for

this document, hence the majority carriers are electrons.

Figure 10 shows the band structure of an n-type semiconductor alongside the band

structure of a metal. E_0 is the free space energy level or vacuum level, the zero electron

energy level immediately outside the material. E_c and E_v are the energy levels of the

conduction band and the valence band respectively (recall that in metals there is no band

gap because E_c and E_v overlap, hence, their levels are ignored in this situation), and E_{fs}

and E_{fm} are the Fermi levels of the semiconductor and the metal respectively. The

difference between the vacuum level and the Fermi level determines the work functions

of the metal, ϕ_m, and the semiconductor, ϕ_s [11]. The electron affinity, χ, of the

semiconductor is the minimum energy required to move an electron from the bottom of

the conduction band, E_c, to the vacuum level [11]. Notice that the Fermi levels of the two

materials are unequal. Also notice that the Fermi level in the semiconductor is within the

band gap (i.e. the forbidden region) of the energy spectrum.

metal   **n-type semiconductor**
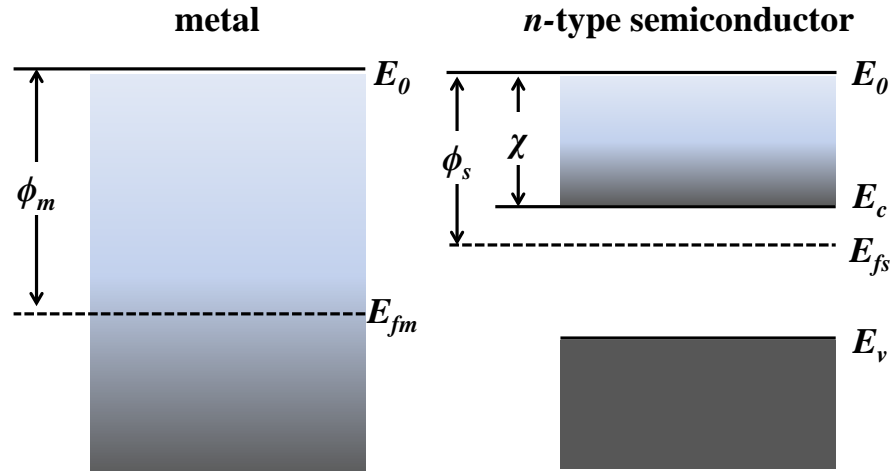
Figure 10. Band structure of disjoined metal and semiconductor.

A Word on the Fermi Level

The Fermi level describes the highest occupied energy level of the collection of
electrons at absolute zero temperature [9]. It is determined by Fermi-Dirac statistics and
the Pauli Exclusion Principle, which states that electrons (or fermions) cannot coexist in
identical energy states. So at absolute zero, they occupy the lowest available energy
states, the highest of which can be considered the "surface of the Fermi Sea of electrons"
[11]. The Fermi energy is a critical concept in the field of solid state physics for
understanding thermal and electrical properties. Energy from many processes cannot be
imparted to most of the electrons because there are no available energy states for them to
transition to within a fraction of an electron volt from their present energy.

The Pauli Exclusion Principle requires the existence of energy band gaps in a
crystal lattice. Without the application of the Pauli Exclusion Principle, an electron at the
Fermi level of one atomic site would be permitted to share the energy level with a Fermi
level electron at an adjacent site. But this is not permitted due to the close proximity of

30

the two adjacent lattice sites. So the electrons must occupy higher energy states if all the states below them are filled. The higher energy states would simply constitute the partially filled band found in metals. In the crystal lattice of a semiconductor, however, additional energy would be required to promote electrons into the conduction band. Introducing dopants to the material can move the location of the Fermi level in energy band diagrams [9], which is of great importance because the location of the Fermi level with relation to the conduction band is a major factor in determining the electrical properties of a material [9, 10,11].

Ideal Metal-Semiconductor Junctions

When the metal and the semiconductor are joined, a depletion region is formed similar to that of a *p-n* diode [11]. Recall that the Fermi levels of the two materials do not match, indicating that the average energy of the electrons in one material is lower than the average energy in the other. In the case of the n-type material in Figure 10, the electrons in the metal are generally lower energy than the semiconductor. So the higher energy electrons in the semiconductor diffuse across the junction to the surface of the metal leaving behind positively charged ionized donor sites [11]. An electric field results between the negative surface charge on the metal and the positive ionizations in the semiconductor, and this electric field inhibits any further electron movement across the junction [11]. Ultimately, the ionized layer in the semiconductor constitutes the depletion region as it is "depleted" of free electrons.

Figure 11 shows an ideal junction between a metal and a semiconductor. At the top is a mere visual representation of the depletion region after the electrons in the *n-*

31

type semiconductor have diffused to the surface of the metal leaving behind positively charged ions near the junction. Below that, the charge density distribution, $\rho(x)$, can be seen. Note that the region where the electrons accumulate at the surface of the metal is relatively thin compared to the ionized region of the semiconductor. This is because the positively ionized atoms remain fixed at their lattice sites within the material whereas the electrons in the metal are "free" to accumulate at the surface. Commensurate to the charge distribution one can see a plot of the electric field, $E(x)$. Finally, and most importantly, the bottom of the figure shows the new shape of the energy band diagram that results from the metal-semiconductor junction. In this band diagram, the all-important Schottky barrier height, ϕ_b, is shown as the difference between the bottom of the conduction band and the Fermi level [11]. The shape of the energy band diagram is dictated by three "rules".

1. The Fermi level must be constant throughout the system of both materials when in equilibrium.
2. The electron affinity, χ, must be constant.
3. The vacuum level, E_0, must continuous but not necessarily constant.
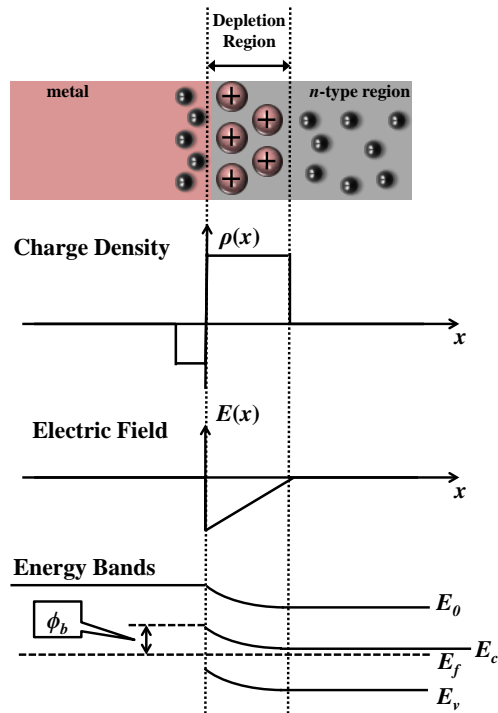
Figure 11. Diagram of band structure leading to the Schottky junction. Below the illustration is the donor charge distribution, $\rho(x)$, and the resultant electric field as a function of location is below that. At the bottom, in order to satisfy the three rules, the energy bands are forced to bend revealing the Schottky barrier height.

Non-Ideal Metal-Semiconductor Junctions

Figure 11 shows the ideal junction between a metal and a semiconductor, which provides us with a reasonable theoretical understanding of Schottky diode behavior. Yet no such perfect junction exists in nature [10], and one should bear in mind that Figure 11 serves only to illustrate the long-range variation in the energy band diagram [15]. In reality, it only shows variation in the energy bands as they approach the junction. What the illustration neglects is the interface specific region (ISR); an extremely thin region on the order of about 1 nm (see Figure 12) [15]. The ISR proves to

be fairly important because it is the region where the magnitude of the SBH is actually determined.
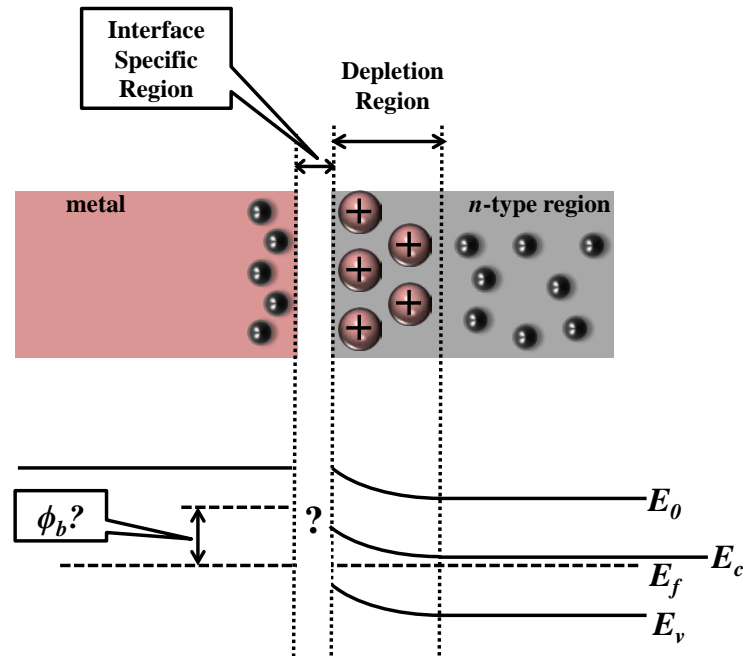
Figure 12. Exaggerated depiction of the interface specific region. The ISR is where the SBH is determined, thus the magnitude of the SBH is subject to considerable error in predicting its actual value mathematically.

One of the first theories of the formation of the Schottky barrier was the Schottky-Mott theory, which proposed that the magnitude of the SBH strongly depended upon the work function of the metal. Indeed, experimental results showed metals with higher work functions *generally* correlated to higher barrier heights, but the dependence was weaker than the Schottky-Mott theory predicted. Confounding the experimental results were indications that material preparation of the metal-semiconductor interface significantly impacted the results. The weak dependence of the SBH on the work

function of the metal was then often explained by theorists as a result of *Fermi level pinning* [15].

Fermi level pinning

While the electronic states within the bulk of a crystal lattice remain constant, the states at the surface, where the crystal lattice is terminated, can be significantly different. These surface specific states can be in the form of true states where the peaks of the wave functions reside at the surface and decrease in amplitude going away from the surface in either direction; into or out of the semiconductor [16]. Alternatively, the surface states may couple with the states of the bulk material creating an increased amplitude at the surface of the material; i.e. a resonant state [16]. The surface specific states are significant contributors to the atomic structure at the surface of the material whereby the atomic structure changes as a result of minimizing the surface energy [9]. All matter has surface specific states. In the case of metals, the states create dipoles that affect the work function of the metal. In the case of semiconductors, surface states that fall within the band gap of the bulk material are thought to "pin" the Fermi level position [15]. But in the case where the surface states are not within the band gap, the pinning of the Fermi level does not occur. Such is the case with non-polar III-V semiconductors like the GaN material being worked with in this research. Ultimately, there is not much band bending on some cleaved non-polar surfaces [15].

The *charge neutrality concept* lies at the heart of Fermi level pinning [11]. The charge neutrality concept says that at absolute zero, the surface states will fill from the lowest energy level up to the Fermi level. If this Fermi level happens to be below the

charge neutrality level, then the surface of the material will be positively charged. If the Fermi level equals the charge neutrality level, the surface of the semiconductor will be electrically neutral. So it follows that if the Fermi level is above the charge neutrality level, the surface of the semiconductor will be electrically negative. Recall the first rule from the three rules governing the shape of the energy band diagram, "The Fermi level must be constant throughout the system of both materials when in equilibrium." This means that the charge neutrality level permits a unique correspondence between the population of the surface states and the band bending at the surface of the material [11].

Naturally, we want to know where the Fermi level is pinned because the SBH depends on the location of the Fermi level (reference Figure 13). To calculate where the Fermi level is pinned, we make two assumptions. The first assumption is that the density of surface states is somewhat constant near the charge neutrality level. The second assumption is that we can reference the energy levels of the surface states to the energy bands within the bulk material. Technically, there is no conduction band maximum exactly on the atomic surface of the semiconductor material, so we use the conduction band maximum at a location a few lattice spacings away from the surface as our reference point [15]. The consequence of these two assumptions leads us to a little ambiguity on the charge neutrality level at a metal-semiconductor surface but the determination of the Fermi level pinning point remains reliable.
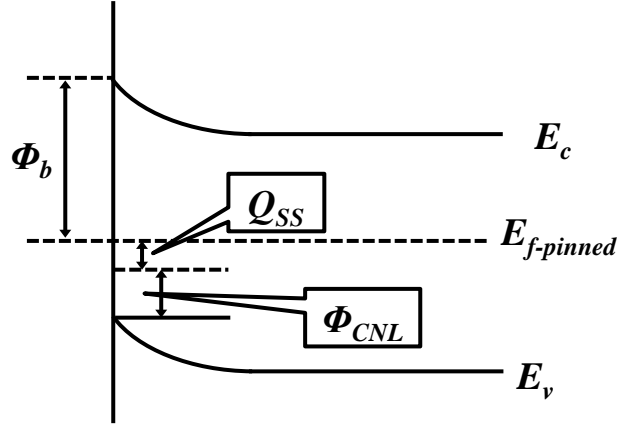
Figure 13. Fermi level pinning band diagram. Due to the surface states a certain amount of surface charge, Q_{SS}, exists above the charge neutrality level, ϕ_{CNL}, at the surface of the semiconductor. This surface charge is thought to contribute to the "pinning" of the Fermi level at the surface of the semiconductor.

To calculate where the Fermi level is pinned, we begin by finding the net charge per unit area at the surface of the material,

$$Q_{SS} = qD_{SS}\left(\phi_b + \phi_{CNL} - E_g\right), \tag{2}$$

where:

Q_{SS} = Net charge per unit area on the surface

q = The charge of an electron

D_{SS} = Density of surface states $\left(\text{\# of states} \times \text{area}^{-1} \times \text{energy}^{-1}\right)$

ϕ_b = Schottky barrier height

ϕ_{CNL} = Charge neutrality level relative to the valence band maximum

E_g = Energy band gap

It should be noted that the SBH, ϕ_b, does not exist in an isolated semiconductor because it is also dependent upon the nature of the metal used in the metal-semiconductor junction [11]. However, for the sake of brevity, we use this symbol as it represents the same quantity. As previously implied, the charge neutrality level of surface states should

37

exactly equal the Fermi level in an intrinsic, undoped, semiconductor. Conversely, doped semiconductors should exhibit some deviation between the charge neutrality level and the surface Fermi level necessary to produce the surface charge that balances the charge arising from exposed dopants in the space charge region. The balance is defined by the following equation, which, incidentally is used to find the pinned Fermi level:

$$0 = qD_{SS}\left(\phi_b + \phi_{CNL} - E_g\right) + \sqrt{2\varepsilon N_D\left(\phi_b - E_{f-pinned}\right)},$$ (3)

where:
N_D = Number of dopants
$E_{f-pinned}$ = The pinned Fermi energy level.

Schottky Barrier Formation

Fermi level pinning became a focal point for describing the Schottky barrier formation for several decades after the inconsistencies between experimental results and the Schottky-Mott theory confounded semiconductor research [15]. As a consequence, many of the theories that followed focused too heavily on the Fermi level pinning phenomenon and neglected the structure of the ISR. It should come as no surprise that the structure in the ISR has an impact on the formation of the Schottky barrier. When the two materials are joined, redistribution of charge occurs due to the overlap of wave functions from the two sides [16]. Bonds are broken. New bonds form, and the ISR takes on a "personality" of its own. So intuitively we expect the charge transfer to be driven by not only the semiconductor (as Fermi level pinning theories suggest) but more so on the electronic states in the ISR. And from a quantum mechanical perspective, this

makes better follows intuition than simply attributing the Schottky barrier formation solely to the characteristics of the semiconductor alone (or the metal for that matter) [15].

Ultimately, it was not until the 1990's that clear evidence emerged confirming what had been suspected; that SBHs at metal to semiconductor junctions were frequently inhomogeneous [15] (see Figure 14). The advent of spatially-resolved techniques such as ballistic electron emission microscopy brought about clear evidence for SBH inhomogeneity. While this was a measureable breakthrough, the question of how the SBH seemed to average out to nearly constant values regardless of the metal if it was supposed to be so sensitive to the structure of the ISR remained. In other words, "how can we get the Fermi level pinning phenomenon to agree with the quantum mechanical bonding picture?"
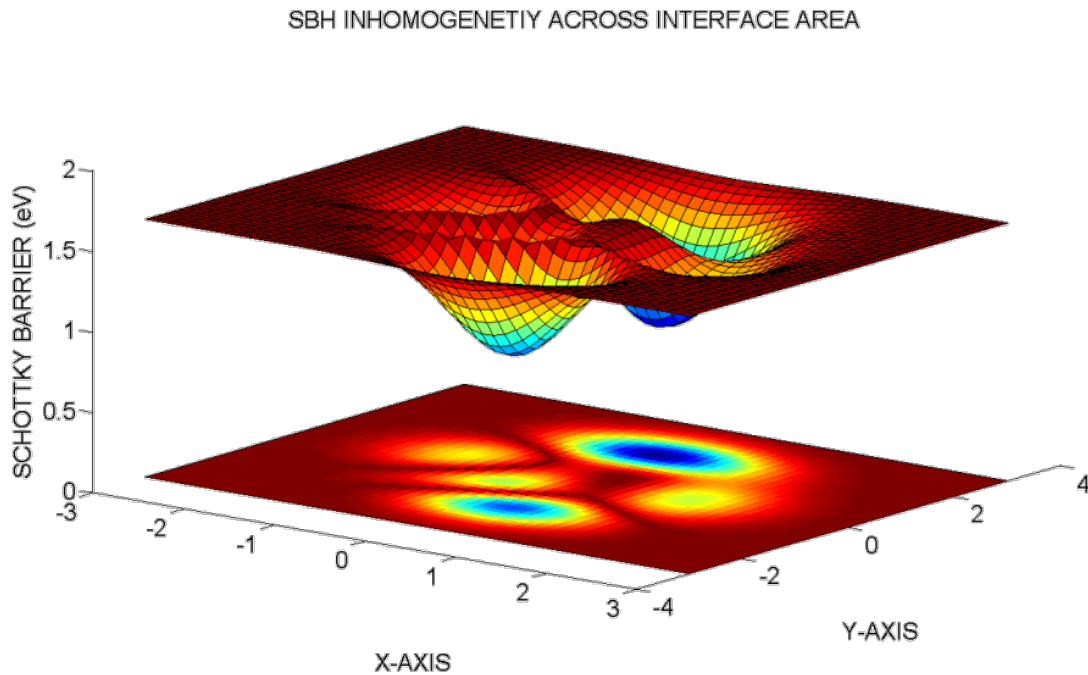
Figure 14. Potential distribution of a low-SBH patch in a high-SBH background.

The apparent answer came about at the turn of the century when molecular physicists used well established methods to model the interface dipole associated with chemical bonding, which showed that "Fermi level pinning was a natural consequence of interfacial bonding" [15]. These findings were further supported through multiple experimentally observed systematic studies [15]. Ultimately, the modern understanding of the formation of the Schottky barrier in metal-semiconductor junctions is based on the structure in the ISR, which creates Fermi level pinning in the natural course of its formation.

2.2.2 Construction

<u>Overview</u>

In the previous section, we determined the SBH was sensitive to the material preparation, which follows intuition when one considers that the SB formation is a function of the atomic structure at the interface. The importance of contact design and material preparation is evidenced by the large body of literature solely devoting itself to the construction methods of Schottky contacts. The sheer number of publications that focus on construction methods implies that the formation of the Schottky barrier is highly sensitive to the method by which the metal-semiconductor junction is formed [17, 18, 19, 20, 21, 22, 23, 24, 25, 26, 27]. Recall that the metal-semiconductor junction often created inhomogeneous Schottky barriers, thus the "name of the game" is to minimize the inhomogeneity of the SBH across the area of the interface between the two materials. The inhomogeneity of the SB arises from inconsistencies in atomic structure in the ISR. An ideal ISR would have a unique but consistent periodic structure that "meshes"

perfectly to the crystal lattice of the bulk material [11]. The inconsistencies in the ISR appear as a result of impurities in the structure or damage to the semiconductor crystal lattice near the surface due to breaking of lattice bonds.

Physical Configuration

In order to measure the electrical properties of a Schottky diode, a complete circuit must be achieved through which the current-voltage (*I-V*) or capacitance-voltage (*C-V*) characteristics can be determined. In the case of a semiconductor thin film, such as the GaN used in this research, two metal contacts are required. The first contact would be the Schottky contact, whose junction to the semiconductor creates the Schottky barrier and is where the actual rectification occurs. The second contact, the *Ohmic contact*, is necessary to complete the circuit through the semiconductor material (see Figure 15). Yet in the case of the thin films being used in this research, the GaN was grown on a sapphire substrate which prohibits putting the contacts on opposite sides of the material. In these situations, it is common practice to put the Ohmic and Schottky contacts on the same side, juxtaposed to each other [17, 18, 19, 20, 21, 22, 23, 24, 25, 26, 27].
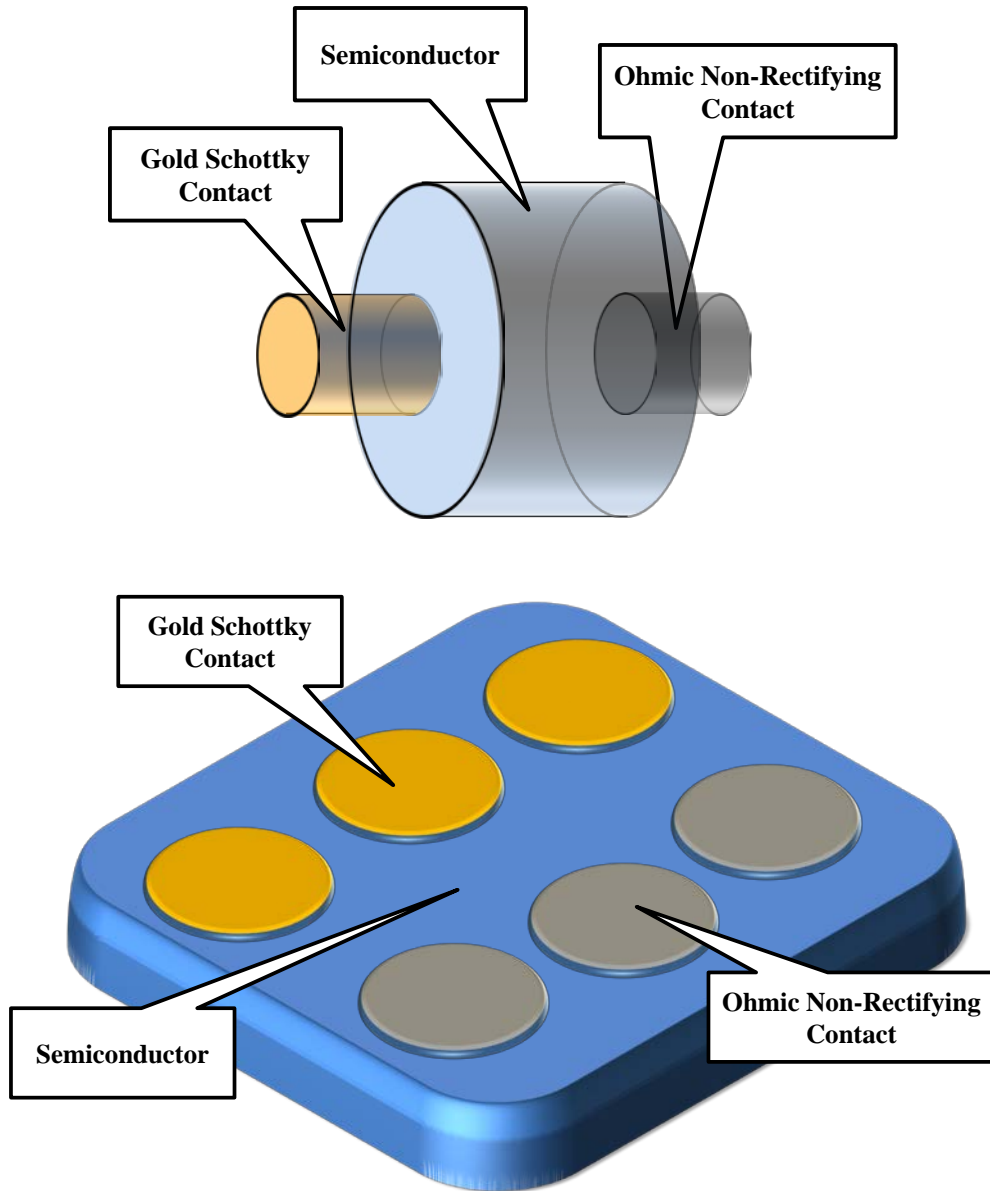
Figure 15. Schottky diode contact arrangement. The top picture shows a "traditional" thru-style configuration where the semiconductor is sandwiched between the Ohmic and Schottky contacts. Below it is the configuration used in this study whereby the contacts are on the same side of the material of the thin film.

Application of Metal Contacts

Because of the sensitivity to material preparation and contamination, the simplest methods of applying metal contacts to a semiconductor surface must be ruled

out. Sputtering molten metal to the surface of the semiconductor would be unwise in that the metal would pick up impurities from the atmosphere, and the heat from the metal would thermally damage many of the lattice bonds at the surface of the semiconductor. Mechanically pressing of metal contacts to the semiconductor also introduces impurities and would likely distress the crystal structure. While some of the crystal structure may be restorable through high temperature annealing, much of the damage may be irreversible [11].

Most techniques used today involve evaporation of the metal under vacuum conditions and allowing the metal vapor to condense on the surface of the semiconductor [17, 19, 20, 22, 23, 24, 27]. The vacuum conditions mitigate contaminants in the system. Likewise a thorough chemical cleaning of the semiconductor surface prior to being placed in the vacuum chamber is warranted [17, 19, 20, 22, 23, 24, 27]. The metal is evaporated thermally, chemically, with lasers, or in the case of this study, with an electron beam. A cloud of dissociated metal atoms forms and subsequently condenses on the surfaces around it. To prevent the entire semiconductor surface from being coated with the metal, a thin metal mask (such as stainless steel) is used to protect the areas of the semiconductor surface of [22, 24, 25, 26]. An example of electron beam vaporization epitaxy is shown in Figure 16.   The localized heat source of the electron beam coupled with the vacuum conditions prevents heat from altering the lattice structure of the semiconductor. This is a proven method used by other semiconductor researchers and was the chosen method in this research [22, 24, 25, 26].
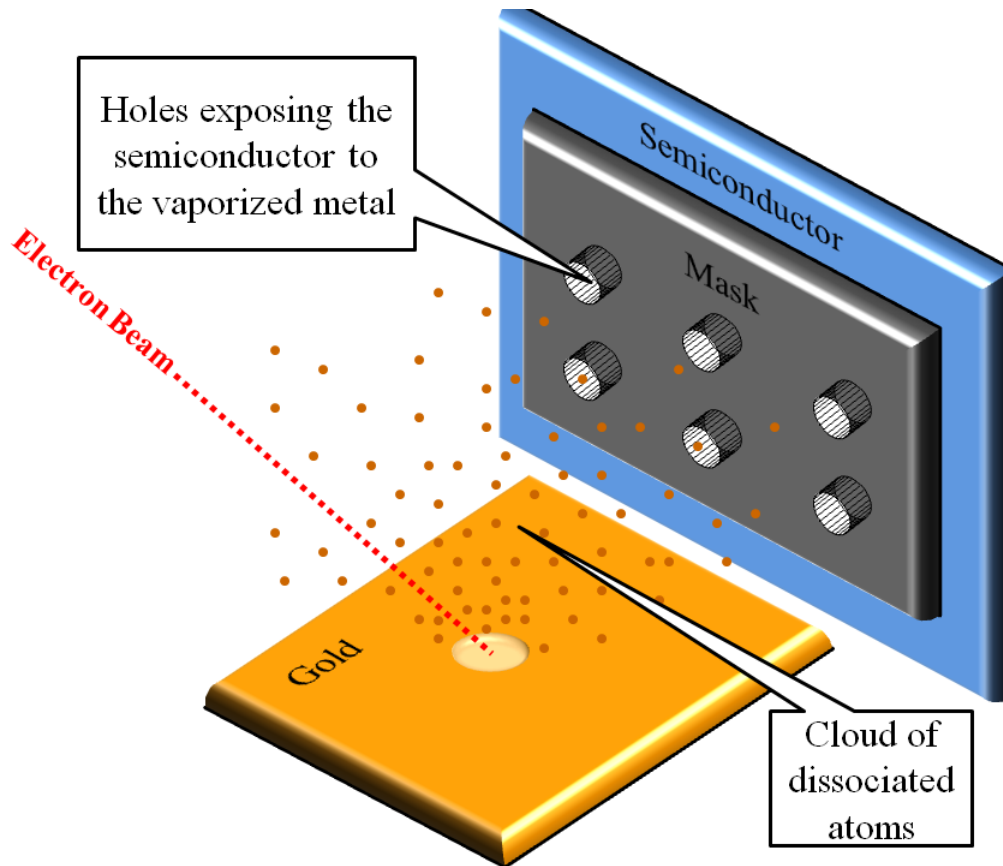
Figure 16. Electron beam vaporization epitaxy. Inside a vacuum chamber, an electron beam focuses on a piece of gold. The dissociated gold atoms float into the chamber and deposit on the surfaces around it. The mask serves to allow the gold to deposit only on the parts of the semiconductor that are desired.

2.2.3 Measuring the Schottky Barrier Height (I-V and I-V-T measurements)

While there are several methods available to measure the SBH of a device, the two primary means used in this study were the current-voltage (*I-V*) measurement technique and the current-voltage-temperature (*I-V-T*) technique. Photoemission spectroscopy was the method used previously by McHale [15], which did not require the application of metal contacts to the rare earth doped thin films. As an extension of his

work, Schottky and Ohmic contacts were formed at the surface of the same RE-doped

thin films used in his study and subsequently *I-V* and *I-V-T* measurements were taken.

I-V Measurement

The *I-V* measurements were the primary means of determining the Schottky

barrier height in this research. To take these measurements, the researcher applies a

range of voltages to the diode and records the corresponding currents. Then, a semi-

logarithmic plot of the current as a function of voltage, such as the one in Figure 17, is

evaluated. Three regions in the plot should emerge. Region I, the region below V_{min}, is

dominated by currents caused by electrons that are thermally excited at or near the SBH

[28] and require little electric potential to drift across the barrier. Region II is where the

effects of the Schottky barrier dominate, and region III is where the series resistance of

the circuit dominates [4, 28].

SEMILOGARITHMIC THEORETICAL SCHOTTKY DIODE FORWARD I-V CURVE

V_{min}

V_{max}

I_S

Extrapolated
line

Amperes

Region I
(Thermionic dominated)

Region II
(Schottky dominated)

Region III
(Series resistance dominated)

Volts
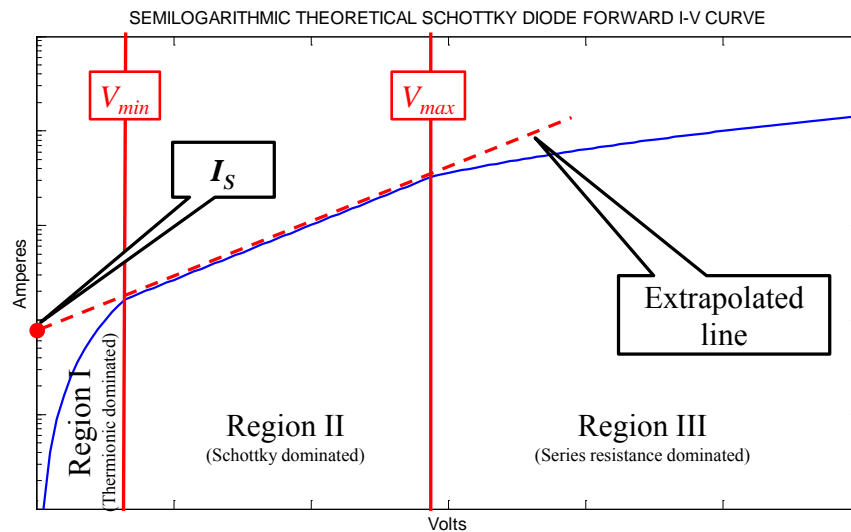
Figure 17. Theoretical semi-logarithmic *I-V* plot for a typical Schottky diode.

45

To better characterize the *I-V* relationship of the diode, a line is extrapolated through region II, and the *y*-axis intercept of this line gives the saturation current, I_S. We can use the value of the saturation current to express the diode current, I_D,

$$I_D \simeq I_S\left(e^{\beta V_D/n} - 1\right),$$ (4)

where:
I_S = The saturation current
$\beta = q/k_bT$
k_b = Boltzmann's constant
V_D = Voltage drop across the diode
n = The ideality factor.

More importantly, the saturation current, I_S, can be used to find the Schottky barrier height by solving equation (5)

$$I_s = AA^{**}T^2 e^{-q\phi_b/k_BT},$$ (5)

solving for ϕ_b...

$$\phi_b = \frac{kT}{q}\ln\left(\frac{AA^{**}T^2}{I_S}\right)$$

where:
A = The area of the contact
A^{**} = The effective Richardson constant.

This method is only as accurate as our knowledge of A^{**}, the effective Richardson constant. A^{**} is the Richardson constant, A^*, multiplied by a factor that accounts for quantum mechanical reflection and optical phonon scattering ($A^* = 4\pi q k_b^2 m^*/h^3 = 120(m^*/m)$A/cm^{2}K^2) [8]. Knowledge of A^{**} can be problematic

46

because it depends on the contact preparation, metal thickness, sample annealing temperatures, and surface cleaning procedures [15]. Note, however, that A^{**} is in the natural logarithm term of Equation (5). Schroder notes than an error of two in A^{**} results in an error of less than k_bT/q in the Schottky barrier, ϕ_b [9]. However, other methods that do not require knowledge of A^{**} can be used to find ϕ_b.

I-V-T Measurement

Norde proposes another method that leverages the temperature dependent nature of the device to determine the barrier height [8]. Norde defines a function, F, as

$$F = \left(\frac{1}{2} - \frac{1}{n}\right)V + \frac{Ir_S}{n}\phi_b \tag{6}$$

where:
$r_S =$ The series resistance of the device.

When this function is plotted against the voltage, V, a minimum value appears, F_{min}, which is used to determine r_s and ϕ_b. The minimum occurs where $dF/dV=0$, yielding a voltage and current corresponding to F_{min}, V_{min}, and I_{min} respectively. So the series resistance is found as

$$r_S = \frac{(2-n)}{I_{min}}\frac{k_BT}{q}. \tag{7}$$

Likewise, the Schottky barrier, ϕ_b, can be found as

$$\phi_b = F_{min} - V_{min}\left(\frac{1}{2} - \frac{1}{n}\right) - \frac{(2-n)}{n}\frac{kT}{q}. \tag{8}$$

However, Equation (6) is derived from Equation (5), which does not get us away from the requirement of knowledge of the effective Richardson constant. To remedy this, Norde presents the *modified Norde* method, given by

$$F1 = \frac{V}{2k_B T / q} - \ln\left(\frac{I}{T^2}\right).$$ (9)

As with the original Norde function, a minimum appears when plotted against *V*. If one were to make several plots of *F1* versus *V* at different temperatures, a unique $F1_{min}$ with corresponding V_{min} and I_{min} values appears at each temperature. We therefore can use Equations (4, 5 and 7) to give a new relationship

$$2F1_{min} + (2-n)\ln\left(\frac{I_{min}}{T^2}\right) = 2 - n\left(\ln\left(AA^{**}\right)+1\right) + \frac{n\phi_b}{k_b T}.$$ (10)

Notice that the charge of an electron, *q*, is not included in the numerator on the right hand side of this equation. This is because *q* is carried in Boltzmann's constant in the denominator and ϕ_b is in units of electron volts.

If we plot the left side of Equation (10) versus $q/k_b T$ a straight line should emerge. The slope of this line should equal $n\phi_b$, and the *y*-axis intercept should be 2-$n[\ln(AA^{**})+1]$. With knowledge of *n* (found from the slope of the semi-logarithmic *I-V* plot) and the area of the contact, *A*, then both the Schottky barrier, ϕ_b, and the effective Richardson constant, A^{**}, can be extracted. The general shape of these plots can be examined for illustrative purposes in Figure 18.
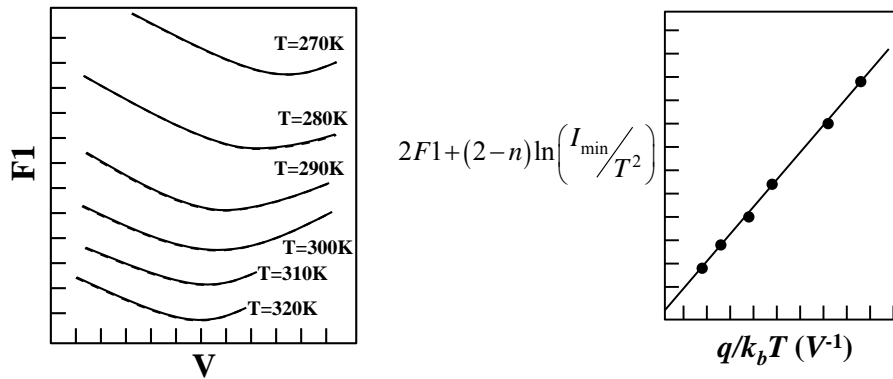
Figure 18. Theoretical modified Norde plots. The figure on the left shows the typical appearance of an _F_1 versus _V_ (normally in mV) plots where the values of $F1_{min}$, V_{min} and I_{min} are found. On the right, the extrapolation to find ϕ_b and A^{**} are extracted.

2.3 Summary

Gadolinium-doped semiconductor diode neutron detectors may not be an achievable means of detecting thermal neutrons emitted from special nuclear materials due to limitations in the associated fields of detector technology. These limitations appear predominantly in the required thickness of the semiconductor material, the necessary bias to achieve a large enough depletion region, and preamplifier noise levels of most commercial preamplifiers [7]. The semiconductor material thickness would need to be on the order of 30-40 μm in order to accommodate the full energy deposition of the 72 or 174keV internal conversion electrons resulting from ^{157}Gd + n capture events, which exceeds current growth capabilities of GaN semiconductor manufacturers. The bias required to achieve a depletion region in this range would need to have a prohibitively large magnitude of 61.2 volts [7]—likely beyond the value at which avalanche breakdown of the current would occur [9]. Finally, the noise levels of typical

49

commercial radiation detection preamplifiers is roughly 0.1-1.2 fC [7]—approaching the charge generated from a single ^{157}Gd neutron capture event (less than 5 fC). Despite these setbacks, present-day interest in the electrical characteristics of rare earth doped GaN exists in the semiconductor device and LED lighting industry as there is a potential for GaN based LEDs that have "tuneable" photoemission via controlled doping of the semiconductor [14]. Additionally, the efficiency of GaN-based diodes may be increased as indicated by McHale's findings of a 25-50% increase in the Schottky barrier heights (SBH) as a result of rare earth doping.

McHale used photoemission spectroscopy to determine the SBH of GaN thin films doped with Yb, Er and Gd. For this research, the same thin films had Schottky contacts and Ohmic contacts applied as shown in Figure 15. These contacts enable two additional methods to validate the photoemission spectroscopy measurements; *I-V* characterization and *I-V-T* characterization. *I-V* characterization is prone to some error due to lack of knowledge of the effective Richardson constant of the diode. The modified Norde method, which has no such requirement [4], can be used to validate the accuracy of the *I-V* measurements and ensure that the estimated effective Richardson constants used were reasonable.

III. Method

3.1 Schottky Contact Design and Construction

3.1.1 Construction Method

As described in Section 2.2.2, the metal contacts were deposited on the GaN thin films using the electron beam vaporization epitaxy facilities at the Air Force Research Laboratories. The films were first cleaned with isopropyl alcohol, followed by acetone, followed by trichloroethylene, followed by a final cleaning of acetone. This was a cleaning method used by previous researchers to a measure of success [27, 29]. After cleaning, a mask was placed over the thin films, and then alternating rows of holes were covered by tape. The thin films were then placed in the electron beam vaporization epitaxy chamber. As shown in Figure 19, the Ohmic contacts were applied under a vacuum of 3×10^{-6} Torr. The Ohmic contacts were composed of 350 Å layer of titanium under a 2300 Å layer of aluminum under a 500 Å layer of nickel under a top layer of 200 Å of gold. Once the metal deposition for the Ohmic contacts was complete, the thin films were removed from the vacuum chamber. The tape was removed from the Schottky contact holes and new tape was applied over the Ohmic contact holes. The thin films were then placed back in the vaporization epitaxy chamber where gold Schottky contacts were deposited to a thickness of 4800 Å (also under vacuum of 3×10^{-6} Torr).
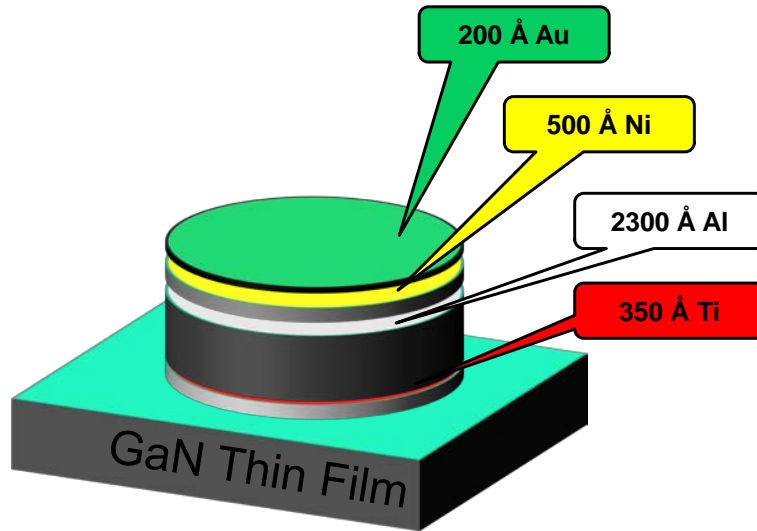
Figure 19. Ohmic contact design.

3.1.2 Initial Design

The first batch of thin films proved useless. They were configured with 2 mm

diameter contacts evenly distributed with 4 mm separations as shown in Figure 20.

Initial *I-V* measurements showed little indication of rectification making them unsuitable

for this research. It was speculated that the size of the contacts were too large; lending

themselves vulnerable to excessive variation in the inhomogeneity in SBHs across the

area of the contact [15]. It was postulated that the variation in the SBH inhomogeneity

was so broad that the lowest regions of the contact approached 0 eV, causing the

Schottky contact to behave similarly to an Ohmic contact. Additionally, it was thought

that the fairly long distance between the contacts, 4 mm, increased the likelihood of

happening upon disruptions in the periodicity of the crystal lattice; interfering with the

conduction of the device via trapping and recombination [9, 10, 11]. So it was decided to

abandon the first batch and construct a different mask with smaller holes arranged in closer proximity to each other specifically designed for the purposes of this research.
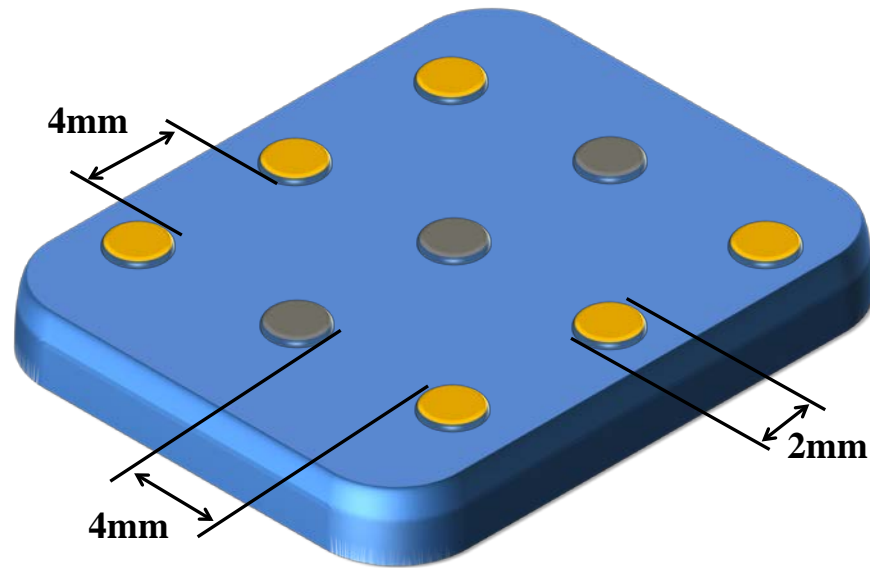
Figure 20. Original Contact configuration.

3.1.3 Final Design

A new mask was built from 0.75 mm thick stainless steel using a computer controlled water jet cutter. The new design featured smaller 1 mm contacts arranged in closer proximity to each other. The cleaning and metal deposition methods remained the same. The relatively short 25 μm proximity between the Schottky and Ohmic contacts made taping over one row of holes without partially masking the adjacent row difficult (see Figure 21). As a consequence some contact pairs were rendered useless due to contamination or poor contact profiles. Some of these contacts, affectionately called "Pac Man" (after the 80's video game) can be seen in Figure 22. However, the new design allowed more diodes (i.e. Schottky-Ohmic contact pairs) to be applied per

individual thin film; increasing the probability of finding a relatively "good" pair of contacts.
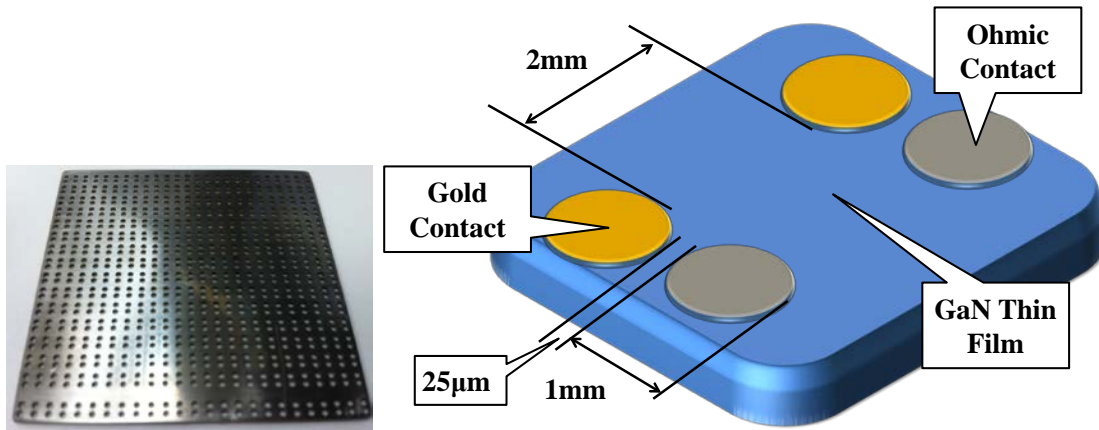
Figure 21. Final contact configuration. Left: A photo of the mask used in the final configuration of the metal contacts. Right: Physical dimensions of the metal contacts

The new configuration produced diodes that exhibited reasonable rectification despite moderate low voltage reverse leakage currents compared to that of commercial, "off the shelf", diodes. The leakage was presumed to be a product of trap assisted tunneling from impurities, field emission tunneling, and hopping conduction [10, 11]. But since the forward current characteristics were the primary region of focus in this research, and the general shape of the curve approximated that of a rectifying diode, the quality of these diodes were considered sufficient to analyze.
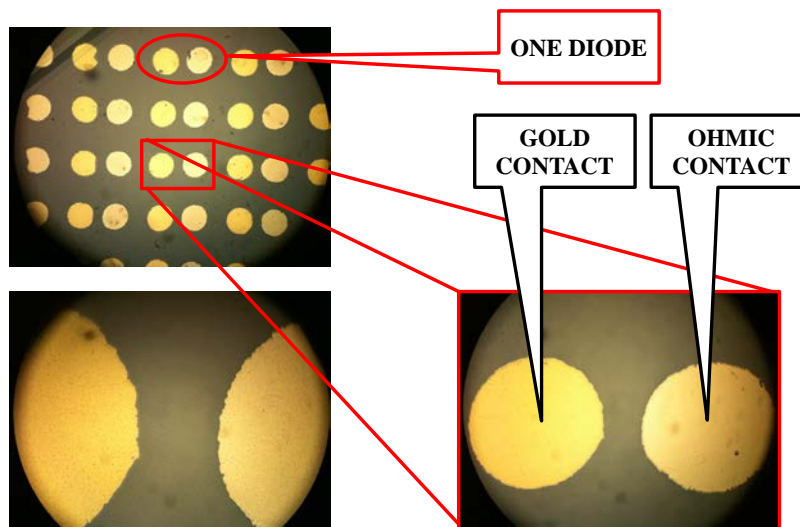
Figure 22. Array of multiple diodes on one thin film. One diode consists of one pair of contacts, a Schottky and an Ohmic contact. Note the "Pac Men" in the upper left corner of the diode array.

3.2 Measurement Techniques

3.2.1 Equipment Configuration

Measurement of the electrical properties of the diodes was accomplished using a Signatone® probe station under a Motic® PSM-1000 microscope. To establish a circuit through the diodes, the Signatone's platinum probes were connected to a Keithley® 237 source measurement unit (SMU) and touched to the contacts' surfaces. The SMU was controlled by a LabView™ program being run in a Dell® Latitude™ E6510 running on the Windows XP® operating system. The first *I-V* measurements were significantly inconsistent among diodes, which was initially attributed to inconsistent deposition of the contacts in the construction process. However, upon further examination, it was determined that the probing technique was to blame.

Properly probing the contact surfaces (see Figure 23) proved critical in gaining usable data. Simply looking through the microscope and lowering the probes to the contact surfaces until physical contact was visually apparent often fractured the contact rendering it unusable. In cases where physical damage was not visually apparent under the microscope, the *I-V* curve would appear similar to that of a simple resistor, and any apparent rectification was lost. As previously discussed, the formation of the interface specific region (ISR) is critical in developing a Schottky barrier. Taking into account the inhomogeneity of the SBH across the area of the contact arising from variations in the atomic structure of the ISR, one might conclude that any damage to the structure of the ISR only further exacerbates the inhomogeneity of the SBH [15]. Thus, it is plausible that the physical pressure of the probe tip to the contact was damaging the atomic structure of the ISR beneath the metal contact. In short, the ISR was far more fragile than expected, and further measures to prevent damage to this region were required.
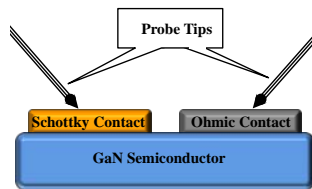
Figure 23. Probe configuration. To complete the circuit, two platinum probes, connected to the SMU, would touch the surfaces of the metal contacts.

3.2.2 Probing Technique and I-V Measurement

To ensure a minimum amount of physical pressure was applied to the contacts by the probe tips, an improved method was used for establishing probe contact. First, a third Ohmic contact near the diode to be measured was designated as a "sacrificial" contact.

Before either of the two probes to be used in measuring the diode were applied, the third

probe was touched to the surface of the sacrificial contact using the previous method of

visual inspection. So long as physical contact was confirmed without visible damage to

the contact, it was deemed to be a "good" probing without regard to any potential damage

incurred to the ISR. Next, a MIN^{TM} DSO201 oscilloscope was tied in series to the circuit

between the third probe on the sacrificial contact and the probe for the Ohmic contact of

the diode. Subsequently a potential difference of 0.5 V (low enough to prevent arcing

and high enough to render measurable currents) was applied to the probes prior to

lowering the second probe to the diode's Ohmic contact. As the second probe was slowly

lowered toward the surface of the diode's Ohmic contact, the oscilloscope would register

"spikes" indicating that probe was responding to the Van Der Waals forces across the air

gap between the probe tip and the diode contact [16]. At this point, the probe, which was

fixed to the end of a thin 12 cm long brass rod, was bouncing back and forth like a spring

board between the Van Der Waals force and the restorative forces of the probe arm;

making and breaking contact with the metal. Once the spiking on the oscilloscope was

observed, the probe would be lowered, even more slowly, until the spiking on the

oscilloscope disappeared and a constant current emerged. This was determined to be the

point at which contact was complete. The same procedure was then performed for

probing the Schottky contact except the Ohmic contact of the diode would be used

instead of the sacrificial contact. This completed the probing process for making *I-V*

measurements. As one might imagine, this probing technique was more of an art than a

science, and it required a significant amount of finesse and practice on the part of the

user. The setup was extremely sensitive to vibrations. Variations in current could be

observed as a results of environmental disturbances as seemingly insignificant as persons in the room stomping their feet or the building heating/ventilation and air conditioning (HVAC) unit turning on or off, thus it was necessary to perform *I-V* measurements with the HVAC unit turned off and nobody in the room.

The *I-V* measurements were taken in "sweep mode" of the SMU, whereby the SMU would record individual current values corresponding to an applied voltage that was incremented in 1 mV steps across a given range. For each voltage step a single mean current was recorded based off of 32 measurements. The measurements were afforded a 16.67 ms integration time. Once the raw data was accumulated, it was passed to Matrix Laboratory[®] for processing and analysis.

3.2.3 I-V-T Measurement Setup

In order to control for variations arising from probing conditions, the *I-V-T* measurements were taken with the probes still in place from the previous *I-V* measurements. To alter the temperature of the diode, the thin film was placed on a stainless steel "island" in a bath of liquid nitrogen (see Figure 24). As the liquid nitrogen evaporated, the temperature of the island slowly increased. The rise in temperature was sufficiently slow; allowing for *I-V* measurement sweeps to be taken at different temperatures with little concern for temperature change from the beginning to the end of the sweep. Pre- and post-measurements of the diode temperature, taken with a Cen-Tech[®] 91778 non-contact laser thermometer, confirmed temperature did not vary by more than 1 K over the course of an *I-V* measurement sweep.
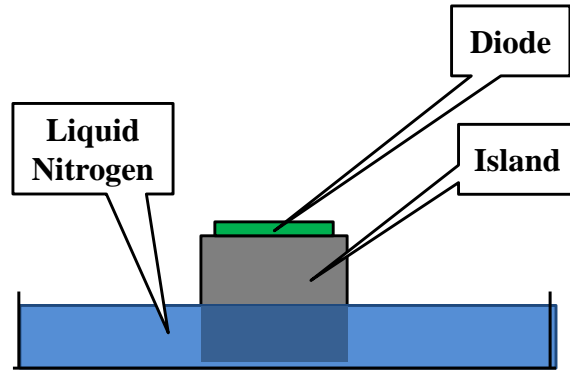
Figure 24. Initial setup for multiple temperatures in *I-V-T* measurements. The thin film was placed on top of the island, surrounded by liquid nitrogen, and probed for *I-V* measurements. As the liquid nitrogen evaporated, the temperature of the island (and consequently the thin diode) would rise, enabling further *I-V* measurements at different temperatures.

Although adequate temperature control of the diode was achieved, an unforeseen problem developed. Humidity in the air condensed on the sample and subsequently froze (see Figure 25). The frost confounded the *I-V* measurements by movemening the probe tips through the expansion of the freezing water. As discussed in the previous section, the pressure applied to the contacts by the probes must be kept to an absolute minimum. Bearing in mind that the probe tips are "barely" touching the contacts, it may come as no surprise that when the water froze, the subsequent expansion lifted the probe away from the surface of the contact. This was confirmed by using the oscilloscope to observe the "spiking" in the current that was observed when the probe was originally placed. In essence, the ice was lifting the probes from the contacts a sufficient distance to result in jumps in current as the probe responded to the Van Der Waals forces between the probe tip and the metal contact [16].

Before evaporation   **1 minute after evaporation**   **2 minutes after evaporation**
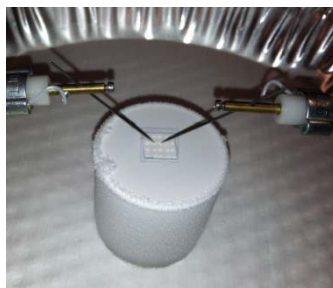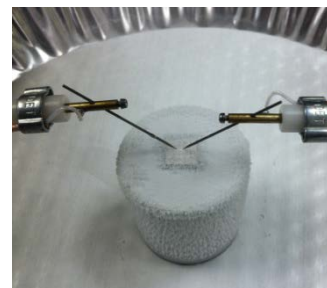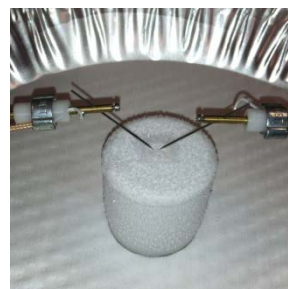
3 minutes after evaporation   **4 minutes after evaporation**

Figure 25. Ice accumulation on the diode. These photos represent a time progression (from left to right, top to bottom) of the ice accumulating on the thin film diode array. The first picture was taken while the liquid nitrogen bath was still evaporating. The subsequent pictures were taken at 1 min time intervals after the last of the liquid nitrogen in the bath had boiled off.

To mitigate this problem, a means to displace atmospheric humidity was needed. As a first (and failed) attempt, a regulated flow of argon shielding gas was circulated over the sample, but the air currents caused probe movements that ruined the *I-V* measurements (the probing was so sensitive that even gently blowing on them would cause changes in measurement). The solution was to set the sample under a curtain of falling N_2 that was evaporating from a second liquid nitrogen bath placed above the sample as shown in Figure 26. This solution remedied the problem as no discernible ice appeared on the sample, and *I-V* data showed no significant disruptions in the measurements.
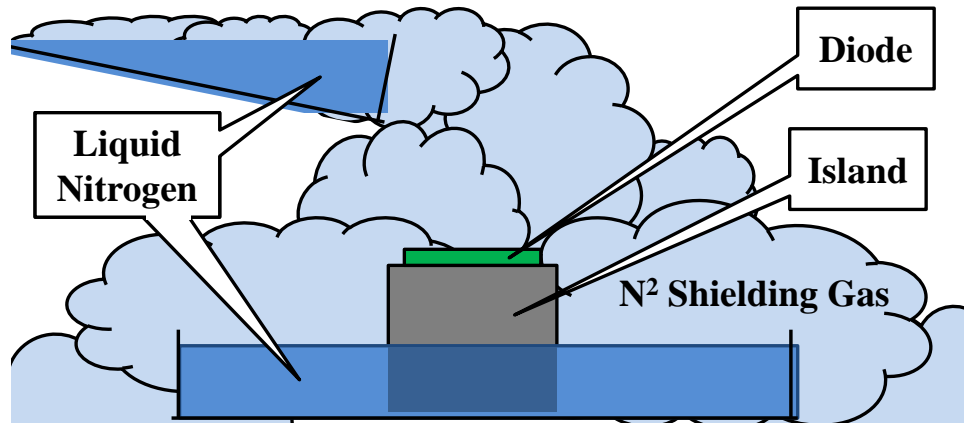
Figure 26. Preventing ice accumulation by shielding the diode with N_2 gas.

In order to minimize temperature changes during a measurement sweep, the sweeps for the *I-V-T* data needed to be considerably faster than the sweeps for the *I-V* data (an *I-V* measurement sweep would take between 30 to 60 min). The results of the *I-V* measurement were used to isolate the relevant region to be used in the modified Norde method [8]. A range of about 0.1 V was identified for each dopant type of diode, and then 23 voltage steps were prescribed for the sweep. Just as before, a single mean current value was recorded from 32 measurements at each voltage step (the same 16.67 ms integration time was also afforded). One sweep was performed for each of six different temperatures; about 240, 250, 260, 270, 280, and 293K.

3.2.4 Summary of Procedure

Before the liquid nitrogen was poured into the bath, the thin film with diode array was placed on top of the island. The probes were then applied to the contacts of a designated diode in accordance with the procedure outlined in Section 3.2.2 using the

DSO201 oscilloscope. At this point, the *I-V* measurements were taken with the SMU

using 1 mV steps across a given range. For each voltage step, the mean current from 32

measurements was recorded. After the *I-V* measurements were taken, the data was

analyzed to find the range over which to sweep the *I-V-T* measurements (about a 0.1V

range). Then with the probes still in place from the *I-V* measurement, liquid nitrogen was

poured into the bath, and *I-V-T* measurements ensued. The intent of leaving the probes in

place was to mitigate inconsistencies between *I-V* measurements and *I-V-T* measurements

arising from variations in setup, probing and environmental conditions. The *I-V-T*

measurement sweeps needed to be relatively fast in order to complete the sweep before

the diode could significantly change temperature, thus only 23 voltage values were set for

the SMU to sweep through. Just as before, the mean current from 32 measurements was

recorded for each voltage step. *I-V-T* measurements were taken at six diode

temperatures. After completing all measurements, the sample was allowed to return to

room temperature before removal from the probe station. Finally, the collected raw data

from the measurements were passed to Matrix Laboratory® for processing.

IV. Results and Analysis

4.1 *I-V* Measurement Initial Results

The results of the first measurements were performed on the Er-doped diodes. As Figure 27 shows, rectification was clearly occurring as the magnitude of the current under 3 V forward bias was nearly ten times that of the current at 3 V reverse bias. Additionally, as one would hope to see, a relatively linear region appeared in the semi-logarithmic plot of the forward bias. Recall from section 2.2.3 that we seek to extrapolate through this linear region to find the saturation current, I_S, so that we may solve for the Schottky barrier height (SBH) via Equation (5). Doing so rendered a *y*-intercept of about 6.6×10^{-9} Amperes.

The next step was to compare this result to expected result based on McHale's findings [7]. Using Equation (5),

$$I_s = AA^{**}T^2 e^{-q\phi_b/k_B T},$$

the following assumptions were made.

$$A \simeq \text{(the area of the contact) } 0.007854 \text{ cm}^2$$

$$A^{**} = \text{(Effective Richardson Constant) } 0.2 \frac{A}{cm^2 \times K^2}$$

$$T = 300K$$

$$\phi_{B,n} = 1.64eV \text{ (Based on McHale's findings)}$$

$$k_B = \text{Boltzmann's Constant.}$$
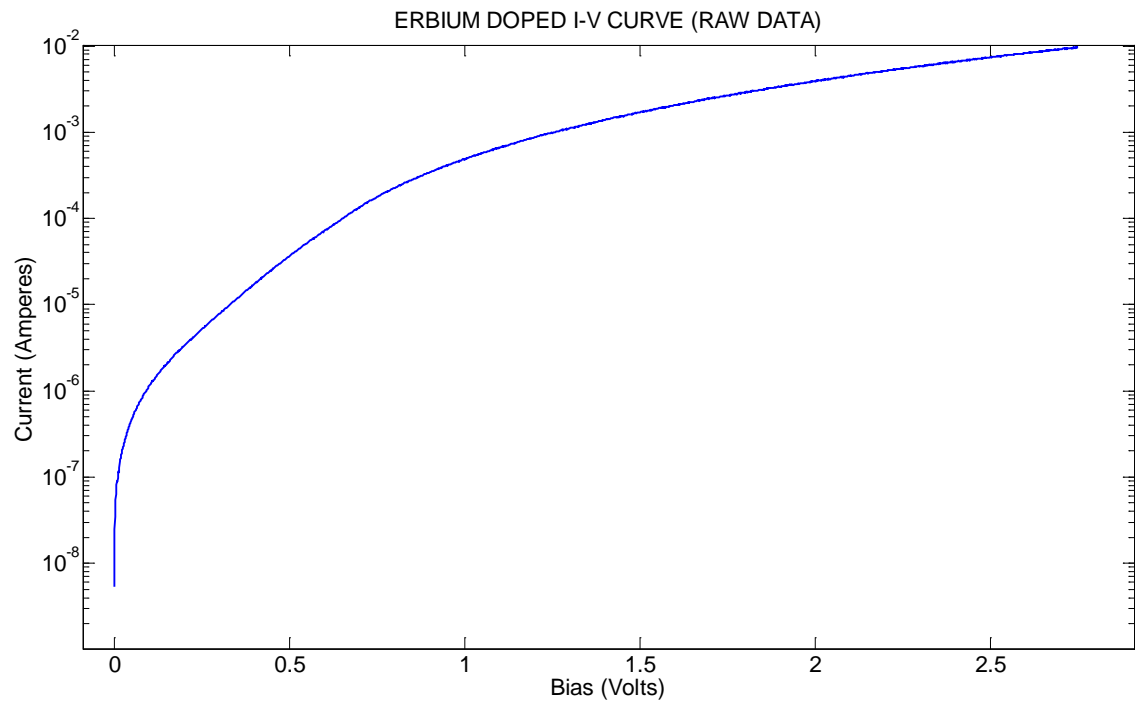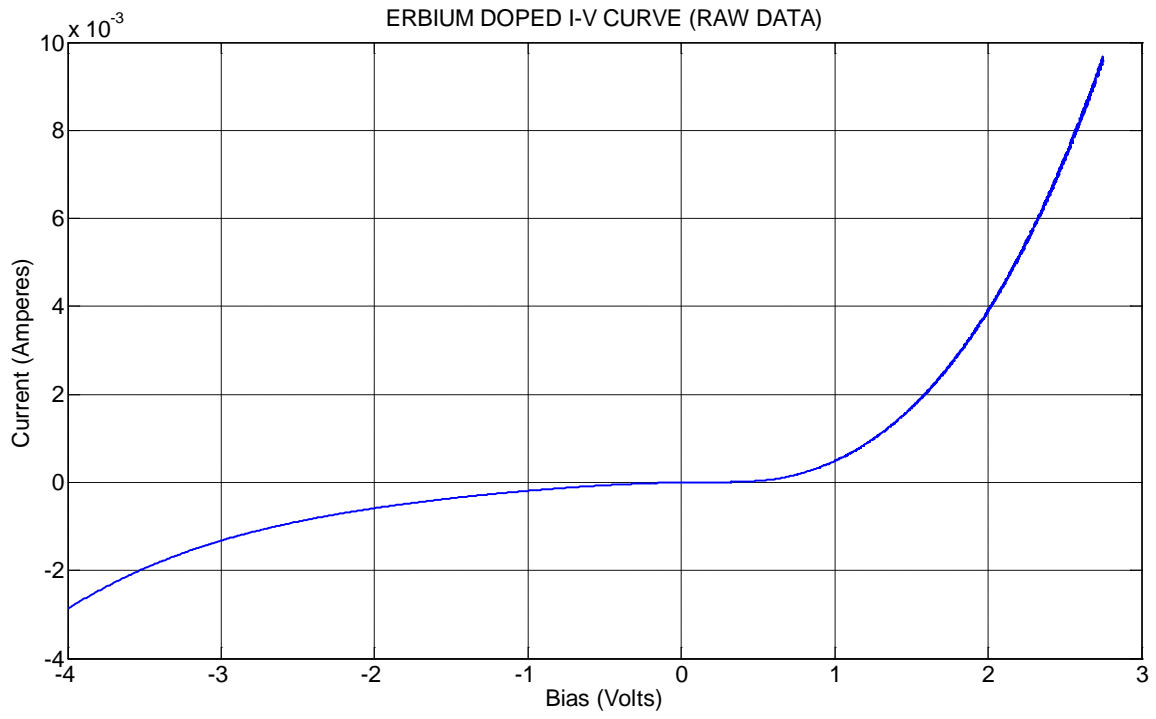
Figure 27. Erbium-doped *I-V* curve data.

The effective Richardson constant was determined as a compromise between the theoretical value of 26 A×cm^{-2}×K^{-2} [19, 24] and experimentally determined values near 0.001 A×cm^{-2}×K^{-2} [17, 18, 20, 24] of undoped GaN. Ultimately, the expected value of the saturation current was I_S=9.94×10^{-28} Amperes. The difference between the calculated and the expected saturation current was 19 orders of magnitude.

A difference of this magnitude could not simply be dismissed as a poor selection of the effective Richardson constant. Assuming the expected saturation current to be true, and holding all other assumptions above to be true, then the effective Richardson constant would be roughly A^{**}=3.3×10^{16} A×cm^{-2}×K^{-2}. Considering a bolt of lightning is only a few hundred kiloAmperes [30], this was an unlikely value for A^{**}. If one went back to the original assumption that A^{**}=0.2 A×cm^{-2}×K^{-2} was reasonable, then either the area of the contact, A, was actually over 5 km^2 (obviously not the case) or the Schottky barrier height, ϕ_b, was 0.52 eV. This last conclusion, was deemed more likely when considering the phenomena of inhomogeneity of the SBH across contact areas. This would mean that if McHale's photoemission spectroscopy measured value of 1.65 eV was accurate, then there was greater than 68% reduction in the SBH. Recall that the variation in the inhomogeneity of the SBH is strongly related to variations in the atomic structure in the ISR [11]. Considering the measures taken to preserve the integrity of ISR (see Section 3.2.2), it seemed doubtful that such a large reduction in the SBH would occur. Yet the evidence spoke to the contrary. So the question remained, "Why were the results of this measurement so inconsistent with McHale's results?"

Up until this point in the research, one very critical (and very incorrect) assumption was made. The assumption was that these were nearly ideal diodes, $n \simeq 1$. This is an assumption that has been proven to be erroneous even in the case of dealing with many commercial diodes [28]. At this point, all further measurements were halted until a method for dealing with non-ideal Schottky diodes could be established.

4.2 *I-V* Measurements Final Results (Dealing With Non-Ideal Diodes)

4.2.1 The Effects of n in Non-Ideal Diodes

Thermionic emission or diffusion models [11] permit the traditional method of determining the SBH of diodes based on an assumption of $n \simeq 1$ in Equation (4),

$$I_D \simeq I_S \left(e^{\beta V_D / n} - 1 \right).$$

In such a case, the ln(I) versus V would reveal a linear region under forward bias through which an extrapolation to the *y*-intercept would reveal the saturation current, I_S. However, for diodes where $n > 1$ no information about the SBH can be given using these methods [10, 28].

Recall from Figure 17 in Section 2.2.3 (provided again below for convenience) that there are three regions in the semi-logarithmic forward bias *I-V* curve of a typical Schottky diode. Region I differs from linearity due to the non-exponential behavior of Schottky diodes at low voltages, and the Cibilis *et. al* defines the relative error of Region I as

66

$$e_m = \frac{I_S e^{\beta V_D/n} - I_S\left(e^{\beta V_D/n} - 1\right)}{I_S\left(e^{\beta V_D/n} - 1\right)}, \tag{11}$$

where V_D can subsequently be defined as

$$V_D = \frac{n}{\beta}\ln\left(\frac{e_{m+1}}{e_m}\right). \tag{12}$$

So if we make $e_m=0.01$ (and consequently $e_{m+1}=0.85$) for $V_D=V_{Dmin}$; we assume $T=300$ K, and we neglect series resistance in the diode, it can be seen that at V_{min}

$$V_{min} \simeq V_{Dmin} = 0.115n, \tag{13}$$

which reveals that the ideality factor strongly impacts the upper limit of Region I [28]. The consequence of this is that if the ideality factor of the diode is large, then the size of Region I will increase. This may not be of consequence so long as the size of Region II does not shrink as a result because Region II is the only region of interest for extrapolation to I_S. It shall be shown, however, that this is often not the case.

SEMILOGARITHMIC THEORETICAL SCHOTTKY DIODE FORWARD I-V CURVE
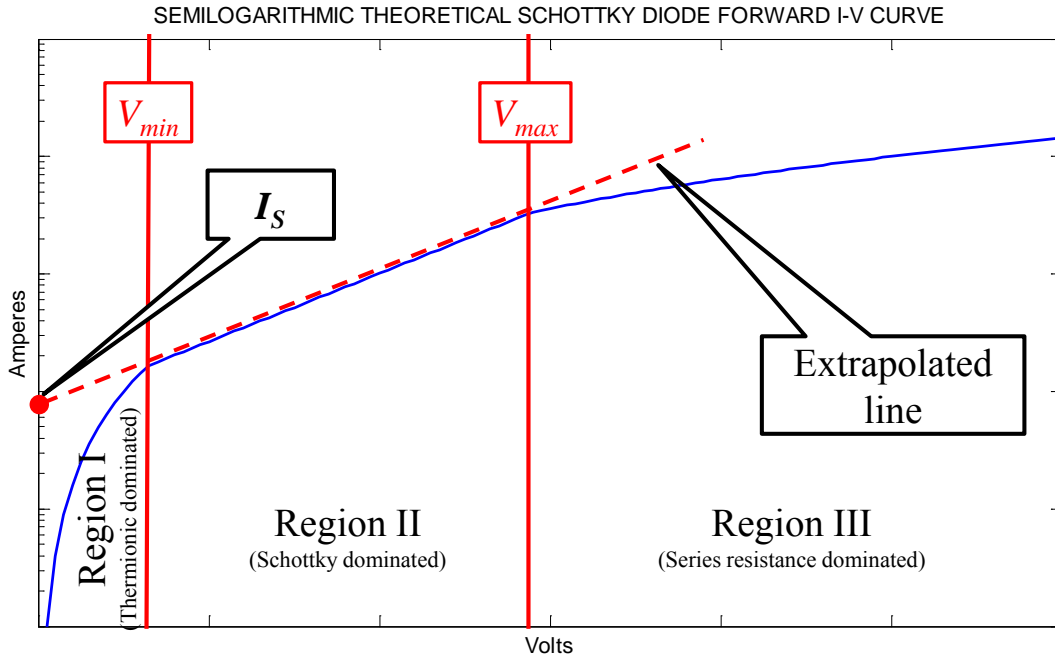
In order to prevent Region II from shrinking when Region I expands, the value of V_{max} must increase. Now looking at Region III, which deviates from linearity due to series resistance in the circuit, the lower limit of Region III, V_{max}. Cibilis *et. al* defines the relative error for nonlinearity as

$$e_M = \frac{I_S\left(e^{\beta V/n} - 1\right) - I_S\left(e^{\beta(V-IR)/n} - 1\right)}{I_S\left(e^{\beta(V-IR)/n} - 1\right)} \tag{14}$$

where:
   $V =$ Total voltage drop the circuit including over series resistance
   $I =$ Total current
   $R =$ series resistance in the circuit.

From Equation (14) the following relationship emerges:

68

$$e^{\beta IR/n} = \frac{e_M + 1}{1 + e_M e^{-\beta V/n}}.$$

From the above equation, since e_M is always less than unity, $e_M e^{-\beta V/n} < 1$ for all

forward bias conditions [28], we neglect this term in the above equation and solve for the

current. The result is

$$I = \frac{n}{\beta R} \ln(e_M + 1). \tag{15}$$

Since Equation (4) gives the diode I-V relationship in terms of relative error, we use

Equation (15) to give

$$V_D \simeq \frac{n}{\beta} \ln\left(1 + \frac{n}{\beta R I_S} \ln(e_M + 1)\right). \tag{16}$$

Just as was done for Region I, if we make e_M=0.01 for V_D=V_{Dmax}; we assume T=300 K

and neglect series resistance in the diode, then at V_{max}

$$V_{max} \simeq V_{Dmax} \simeq 0.025 n \ln\left(1 + \frac{2.5 \times 10^{-4} n}{R I_S}\right). \tag{17}$$

Using Equation (13) and Equation (17) and reasonable values for R and I_S (say

120 Ω and 1 μA respectively) a plot showing the values of V_{min} and V_{max} as a function of

n is shown Figure 28. From the plot it becomes evident that Region II disappears in this

non-ideal diode where $n>1$. V_{min} and V_{max} become inverted, i.e. $V_{min}>V_{max}$.
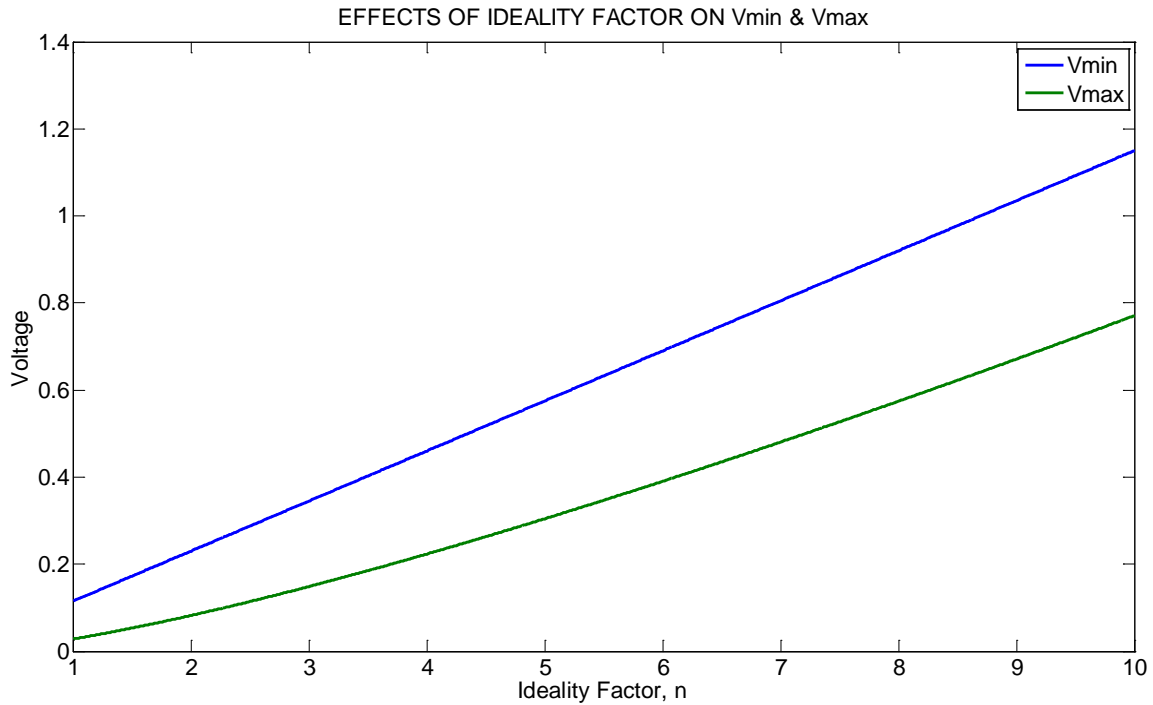
Figure 28. Effects of ideality factor on V_{min} and V_{max} . For a typical series resistance of 120Ω and saturation current 1μA, V_{min} is consistently greater than V_{max} for diodes with an ideality factor $n>1$.

To summarize, a defective ISR gives rise to a non-ideal diode, $n>1$, due to an inhomogeneous SBH across the area of the junction [15]. Consequently, the excessive currents from thermally excited electrons through the low SBH regions confound the Schottky barrier transport current measurements in the low voltage regime of Region II. Additionally, high series resistance confounds the Schottky barrier transport current measurements in the high voltage regime of Region II [28]. The combination of non-ideality and series resistance destroys the linearity of Region II [28], where the Schottky barrier transport mechanism dominates. Without this linearity, an extrapolation to find I_S on the semilogarithmic I-V plot is impossible [10, 28].

4.2.2 Correcting the I-V Curves for Non-Ideal Diodes

In order to address non-ideal diodes accurately, the manner in which the diode was viewed had to be changed. Looking at the diode as a series and parallel resistor circuit equivalent enabled mathematical isolation of the diode while discarding the effects of parallel resistance and series resistance. Figure 29 shows the circuit equivalent of a non-ideal diode. By viewing the diode in this manner, determining the values of I_P, R_P and R_S will lead to a true *I-V* relationship between I_D and V_D.
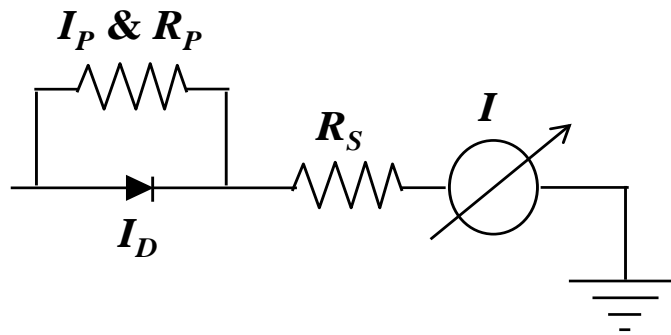
where:
I_P = Parallel current
R_P = Parallel resistance
I_D = Current through the diode
R_S = Series resistance
I = Total current in the circuit

Figure 29. Circuit equivalent of a non-ideal diode. Determining the values of I_P, R_P and R_S from I will enable determination of the true *I-V* relationship.

In this research, three methods of treating the circuit equivalent of the diode were examined [8, 12, 31, 32]. The Norde method assumes an ideality of $n \simeq 1$, so that was immediately discarded as an option. A second method proposed by Lien *et al.* accommodated diodes with higher ideality factors [32], and a third method, proposed by

Jürgen H. Werner [12] was mathematically equivalent to Lien *et al.* The third method

was chosen as it "appears to be the simplest to use and is obviously the most sensitive

method to evidence the contribution of a generation-recombination current" [31].

The first step using the Jürgen Werner method was to determine the value of the

parallel resistance, R_P, which was found by performing a least squares fit to the linear

region of the reverse bias semi-logarithmic *I-V* curve. This least squares fit actually gives

the parallel conductance, G_P, of the diode, but the under the condition that $-eV \gg k_B T$,

then R_P can be found by the relationship

$$R_P = \frac{1}{G_P}.$$

The parallel resistance was found to be 496 Ω, 2,569 Ω and 28,732 Ω for Gd, Er and Yb

respectively.

The next step was to find the current through the diode, I_D. Knowing that the

diode current equals the difference between the total circuit current, *I*, and the parallel

current, I_P, the diode current could be defined

$$I_D = I - I_P$$
$$I_D = I - G_P V.$$

From the diode current, the total conductance of the circuit, *G*, could be found

from the following definition of conductance [10]:

$$G = \frac{dI_D}{dV} = I_D \frac{d \ln(I_D)}{dV}.$$

The total conductance, G, was instrumental in finding the ideality factor, n, and the series resistance, R_S. Under forward bias where $V_D = V - IR_S \gg k_B T / q$, the thermionic diode current could be defined

$$I_D = I_S e^{\frac{\beta}{n}(V - IR_S)}.$$

(18)

For small signal conductance $G = dI_D/dV$ [12], Equation (18) gave

$$\frac{G}{I_D} = \frac{\beta}{n}(1 - GR_S).$$

(19)

Equation (19) facilitated the next step; finding n and R_S. By plotting the conductance divided by the diode current versus the conductance, an extrapolation to the x- and y-intercepts revealed n and R_S. The x-intercept was $1/R_S$ and the y-intercept was β/n. Figure 30 shows the extrapolations of the three different diodes. The ideality factors were 5.972, 10.311 and 10.304 for Gd, Er and Yb respectively. Likewise, the series resistances were 115.78 Ω, 112.05 Ω and 2168.64 Ω for Gd, Er and Yb respectively.
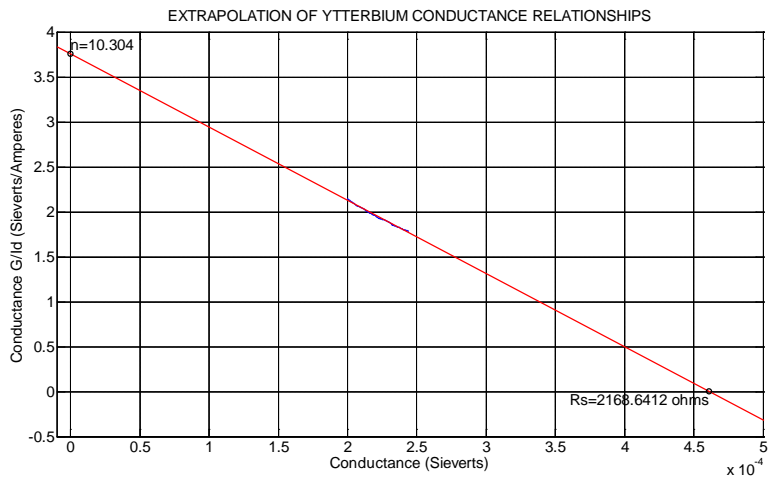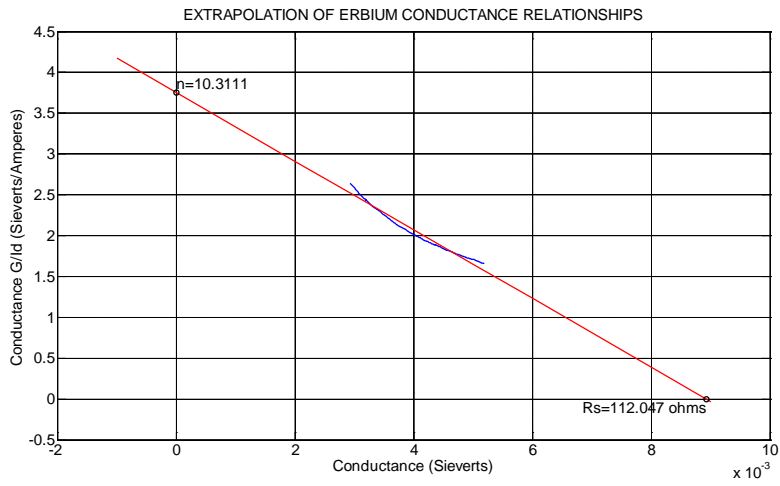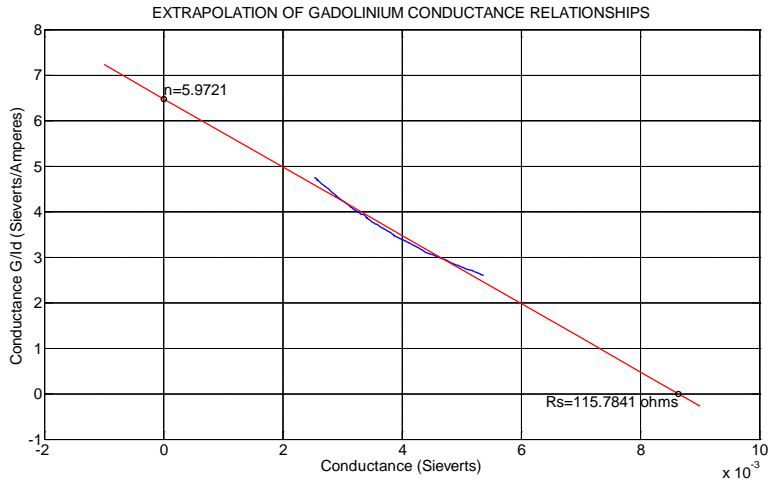
Figure 30. Extrapolations to find *n* and *R_S*.

The last step uses the known values of R_S to find the corrected voltage values, V_{Corr}. The following simple relationship allows for finding V_{Corr} and ultimately leads to a corrected curve that accounts for both the series and parallel resistances of the equivalent circuit:

$$\begin{aligned} V_{Corr} &= V - V_S \\ V_{Corr} &= V - IR_S. \end{aligned} \tag{20}$$

Figure 31 shows semi-logarithmic I-V plots containing the original forward bias curve with two additional curves; one that accounts for parallel resistance and one that accounts for both parallel and series resistance. In all three cases, accounting for the parallel resistance moved the curve to the right and increased the slope at corresponding points. Accounting for both the parallel and series resistances moved the curve slightly back to the left but further increased the slopes at corresponding points. With the new corrected curves an extrapolation to find the saturation current, I_S, seemed more likely to approximate the results found in McHale's work. However, as one can see from the figures there was no apparent linear region in the correct I-V curves through which to extrapolate.
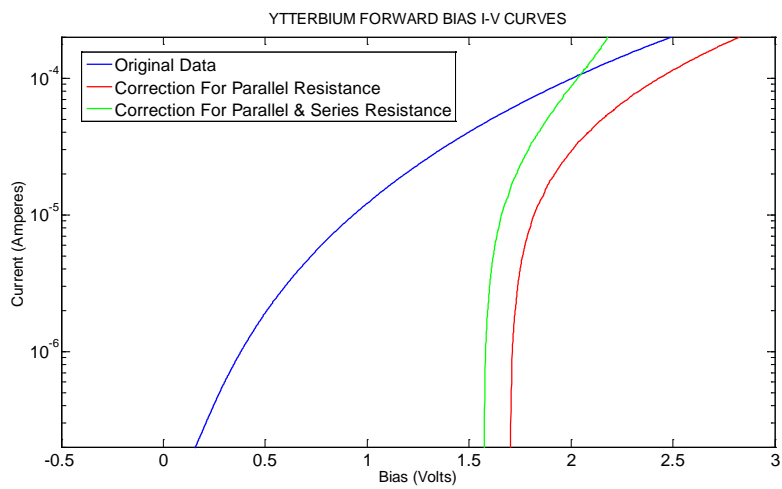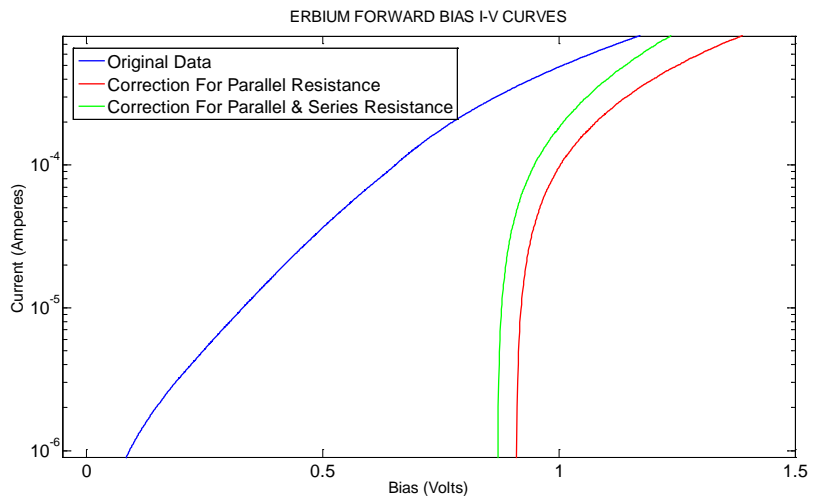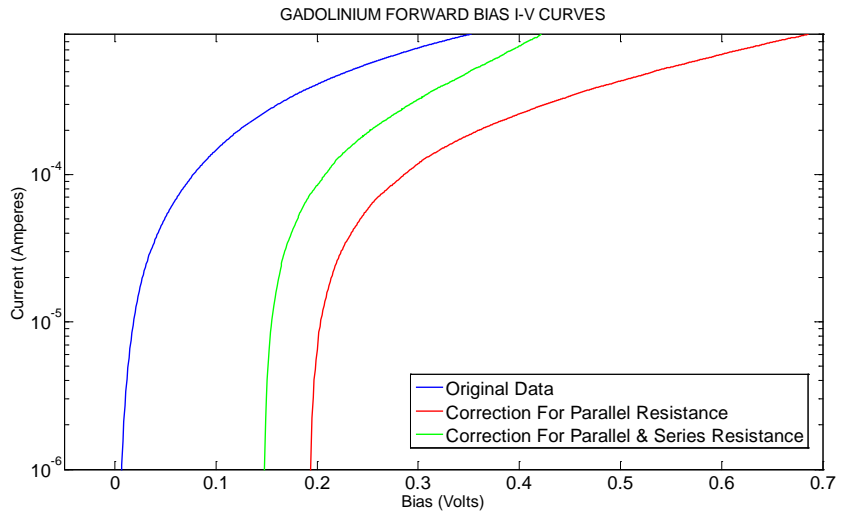
Figure 31. Original and two adjusted forward bias *I-V* curves.

4.2.3 Compensating for Inverted V_{min} and V_{max}

Recall from Figure 17 that the extrapolation to find the saturation current must be through Region II, which, in the case of non-ideal diodes, can disappear as a result of V_{min} and V_{max} inverting (i.e. $V_{max} < V_{min}$). Having known values of n to use in Equation (13) and Equation (17) revealed this was exactly the case for all three dopant types of diodes. To account for this, an iterative MATLAB® program using Equation (13) and Equation (17) was written that incrementally adjusted the value of n until the solutions of both equations matched; finding the point on the curve where $V_{min} \cong V_{max}$. This point was then treated as an infinitesimally small Region II through which to extrapolate. Naturally a true extrapolation was impossible because this was only a point on the curve. So the derivative of the logarithmic curve was taken at this point. The y-axis intercept of the line drawn by the derivative on the semi-logarithmic plot yielded interesting results.

The extrapolations shown in Figure 32 show that the calculated values of the saturation currents are 2.89×10^{-22}, 2.39×10^{-27} and 4.66×10^{-28} A for Gd, Er and Yb respectively. Putting these values of I_S into Equation (5) yields ϕ_b=1.41 eV, ϕ_b=1.71 eV and ϕ_b=1.75 eV for Gd, Er and Yb respectively. These values are reflected in Table 3.
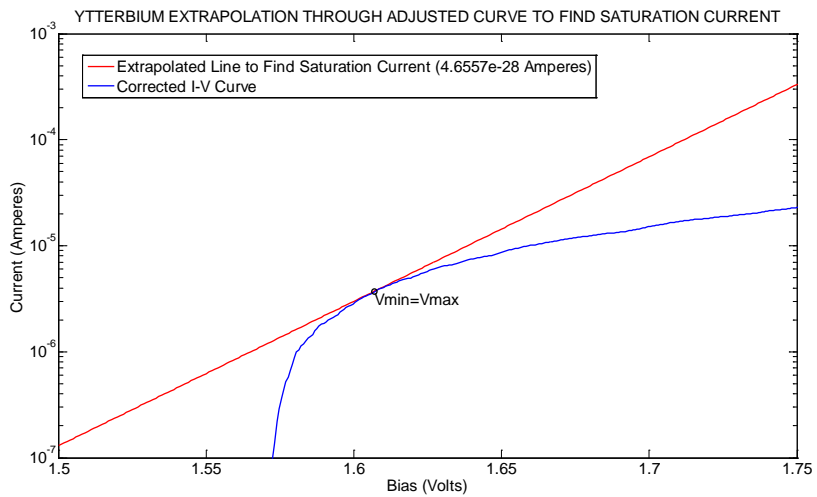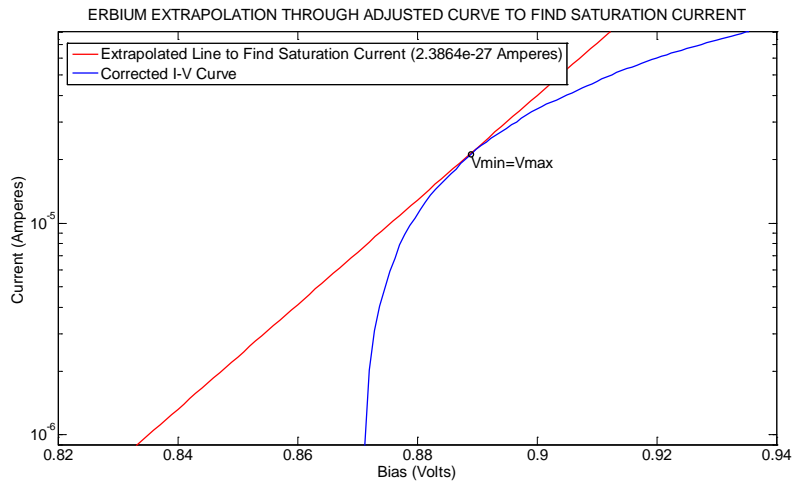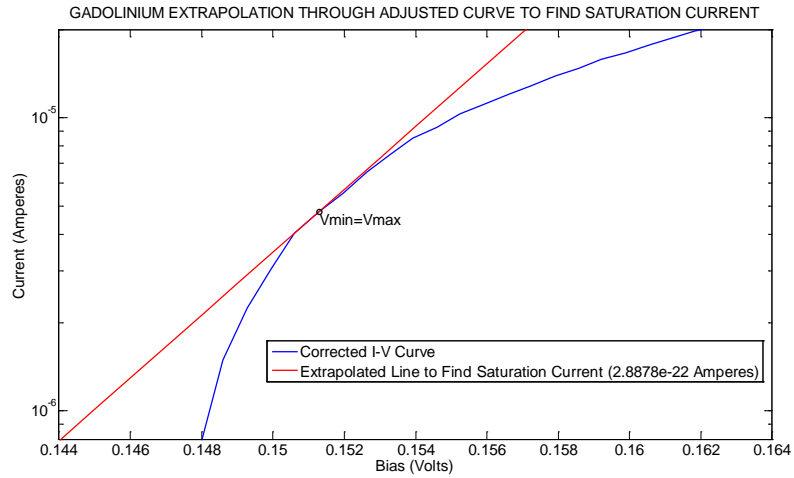
Figure 32. Linear extrapolations to find the saturation current of the diodes.

Table 3. Comparison of Schottky Barrier Height Measurements

Semiconductor Type	^{157}Gd	^{167}Er	^{173}Yb
PE Spectroscopy	1.33±0.1 eV	1.64±0.1 eV	1.68±0.1 eV
I-V Measurements	1.41±0.20 eV	1.71±0.25 eV	1.75±0.28 eV
Max % Deviation	31%	27%	28%

4.2.4 Analysis

Table 3 gives a summary of the Schottky barrier heights calculated from the *I-V* measurements using the Jürgen Werner method. It should be noted statistical error propagation plagued the SBH measurements due to the extensive mathematical processes involved in adjusting the *I-V* curve to account for parallel and series resistances and finding the derivative of the curve at $V_{min}=V_{max}$. The errors in these results were greater than 100% higher than the error in the photoemission spectroscopy measurements made by McHale. The third row in the table shows what the maximum deviation from the photoemission spectroscopy measurements would be if one observed the highest limits of the errors. However, there was reason to speculate that the results were more validating of McHale's measurements if the effective Richardson constant was examined more closely.

The results from the SBH measurements followed the same trends as McHale's photoemission spectroscopy measurements but were universally higher than his. Conveniently neglecting error for the moment, if one considered the assumptions made in these calculations, the effective Richardson constant would return as an issue that must be

dealt with. Recall that knowledge of the effective Richardson constant, A^{**}, is required in order to apply Equation (5)

$$\phi_b = \frac{kT}{q}\ln\left(\frac{AA^{**}T^2}{I_S}\right).$$

A value of 0.2 A×cm^{-2}×K^{-2} was assigned to the effective Richardson constant as a compromise between the theoretical value of 26 A×cm^{-2}×K^{-2} [19, 24] and experimentally determined values near 0.001 A×cm^{-2}×K^{-2} [17, 18, 20, 24] for undoped GaN. Granting that the effective Richardson constant has comparatively little impact because A^{**} is in the numerator of the quotient in the natural logarithm term, it is of considerable interest that an ad hoc reassignment of the value of A^{**} to A^{**}=0.006 A×cm^{-2}×K^{-2} renders results that are within no greater than 2% disagreement with McHale's results across all three types of diode. This revised value of A^{**} is in exact agreement with the experimentally determined results of Hacke et al. [20] who also used gold as a contact material on undoped GaN.

4.3 *I-V-T* Measurements

4.3.1 *Results*

As discussed in Section 2.2.3 the modified Norde function, defined by Equation (9), lent itself well to the *I-V-T* measurements because it had no requirement for prior knowledge of the effective Richardson constant, A^{**},

$$F1 = \frac{V}{2k_BT/q} - \ln\left(\frac{I}{T^2}\right).$$

This function was applied to each of the six *I-V* measurements per dopant type. Figure 33 shows plots of the modified Norde function, *F1*, versus voltage. A clear minimum, *F1min*, emerged from each curve which was then used in a second plot to find the Schottky barrier height, ϕ_b, and the effective Richardson constant, *A***.
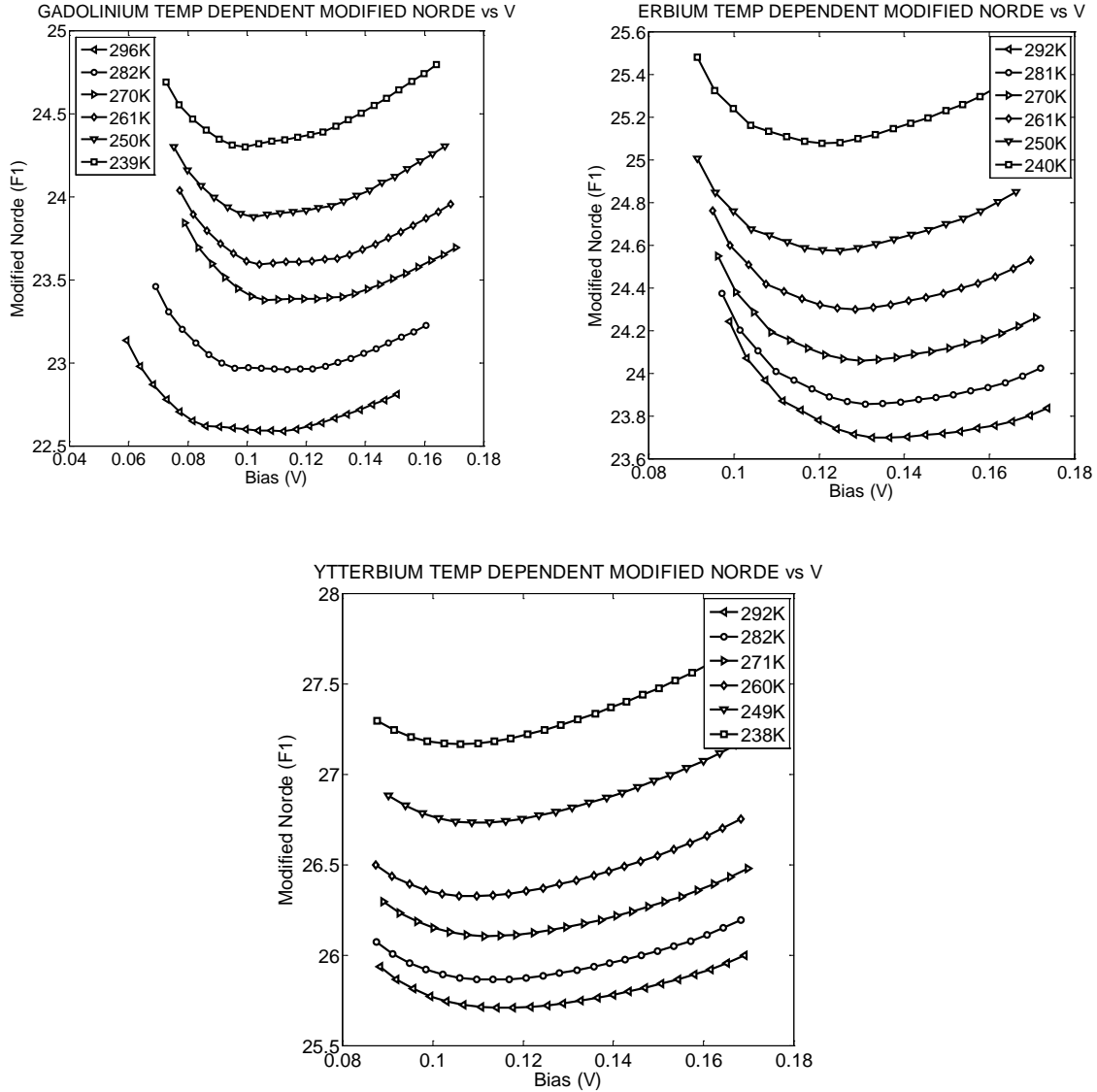
Figure 33. Temperature dependent plots of modified Norde function, *F1* vs *V*.
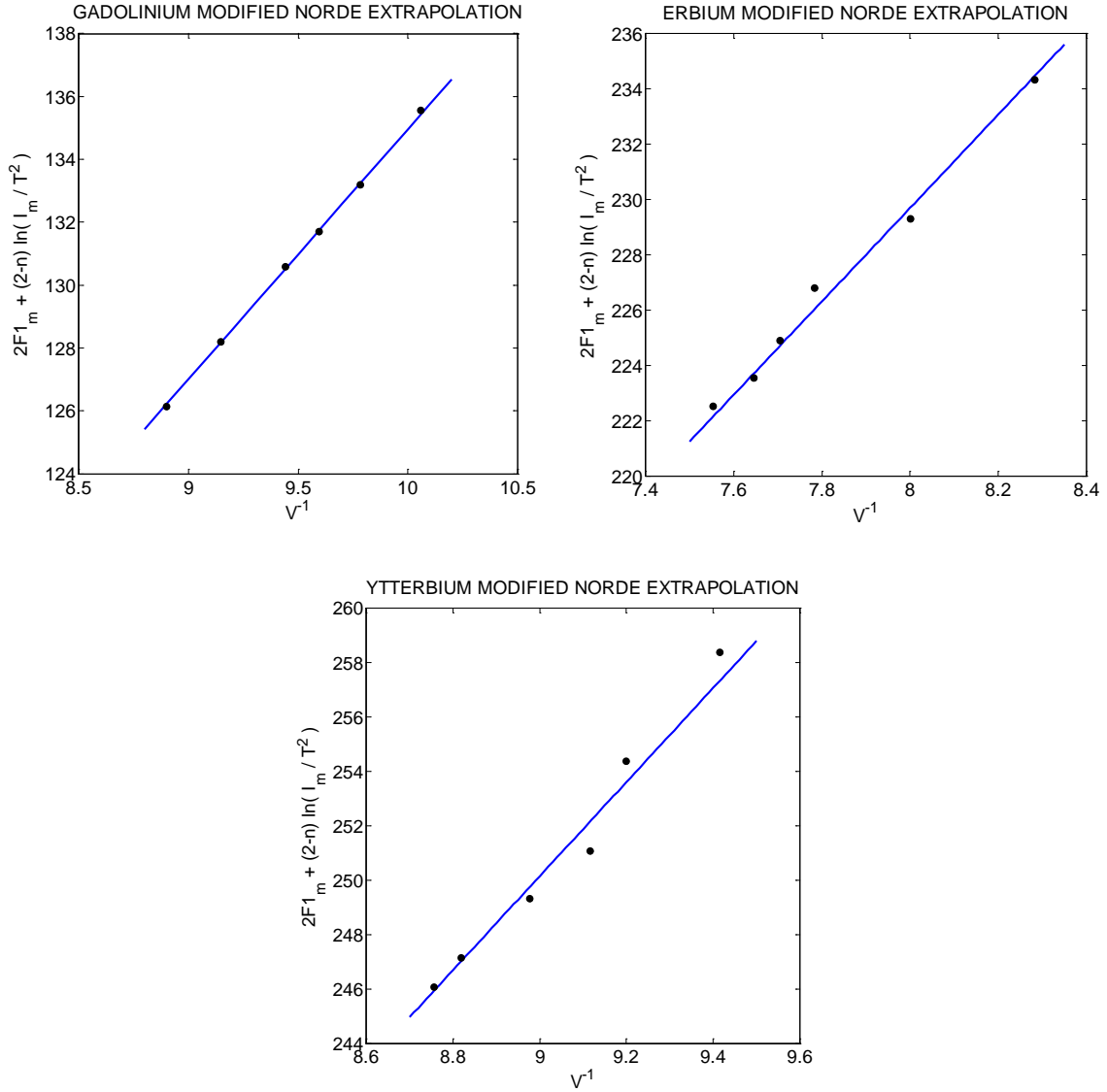
Figure 34. Modified Norde extrapolations to find ϕ_b and A^{**}.

To build the plots in shown in Figure 34, the modified Norde minimums and the corresponding ideality factors (already determined from the previous *I-V* measurements) were put into the left side of Equation (10),

$$2F1_{\min}+\left(2-n\right)\ln\left(\frac{I_{\min}}{T^2}\right)=2-n\left(\ln\left(AA^{**}\right)+1\right)+\frac{n\phi_b}{k_bT}.$$

These values were plotted against q/k_bT (or V^{-1}), which produced a generally linear result. Next, an extrapolation was made through the points, and the slope of the extrapolated line divided by n equalled ϕ_b. Recall that n was determined previously as part of the Jürgen Werner method. Then the y-intercept, which is equal to $2-n\left(\ln\left(AA^{**}\right)+1\right)$, was solved for A^{**}.

The results of the Schottky barrier heights are shown in Table 4, which is an extension of Table 3. Unlike the Jürgen Werner method, the statistical errors propagating through the modified Norde method were more reasonable. The SBH of the Gd-doped diode was 11% lower than McHale's findings, and both the Er-doped and Yb-doped diodes were 15% below his results. Also in the table are the calculated values of A^{**}; gleaned from the y-intercepts in the plot above.

Table 4. Comparison of Schottky Barrier Height Measurements (Complete)

Semiconductor Type		^{157}Gd	^{167}Er	^{173}Yb
ϕ_b	PE Spectroscopy	1.33±0.1 eV	1.64±0.1 eV	1.68±0.1 eV
	I-V Measurement	1.41±0.20 eV	1.71±0.25 eV	1.75±0.28 eV
	I-V-T Measurement	1.19±0.12 eV	1.39±0.16 eV	1.43±0.12 eV
$A^{**}\left(\dfrac{A}{cm^2K^2}\right)$		0.011±0.001	0.036±0.003	0.021±0.002

4.3.2 Analysis

In exactly the opposite fashion as the *I-V* results, the *I-V-T* measurements yielded values for the SBH that were universally lower than McHale's results by 11%, 15% and

15% for Gd, Er and Yb respectively. The mathematical processes involved in obtaining the SBH values afforded a lower error in the results; indicating that these values may be somewhat more accurate. It may also be possible that the SBH values were lower as a result of damage incurred in the ISR from the previous *I-V* measurements. Recall that the *I-V* measurements were taken on the same diodes prior to performing the *I-V-T* measurements and that the *I-V* measurements covered a larger voltage range. In fact, during the *I-V* measurements, it was necessary to exceed the breakdown voltage under reverse bias conditions in order to obtain the data needed for the parallel conductance, G_P. The higher currents associated with the larger magnitude voltages may have damaged the ISR due to Joule heating. One should consider the inhomogeneity of the SBH (see Figure 14). And if one also considers that a corresponding inhomogeneity in current density flows through the contact such that current density is greater in localized regions of low barrier height [15], then the possibility that the ISR was damaged during the previous measurements seems even more plausible. Thus, one can speculate that there is a possibility that the calculated values of the SBH from the *I-V-T* measurements could have been higher if the *I-V-T* measurements were taken before the *I-V* measurements.

One piece of information, garnered from the modified Norde measurements, that the *I-V* measurements couldn't produce was a calculated value of A^{**}. Table 4 also contains this information where it should be noted that values of the effective Richardson constant were higher than previous experimentally determined values on undoped GaN [17, 18, 20, 24]. The calculated values of A^{**} were also on par with the speculated values mentioned in Section 4.2.4. In that section it was observed that adjusting the value

84

of the effective Richardson constant to $A^{**}=0.006$ A$\times$cm$^{-2}\times$K^{-2} renders SBH calculations

that are within no greater than 2% disagreement with McHale's findings across all three

types of diode. A^{**} of the Gd-doped diode came closest to matching this value (a

difference of no more than 0.006 A$\times$cm$^{-2}\times$K^{-2}) followed by the Yb-doped diode and

finally the Er-doped diode. The differences between these values and previous

experimentally determined values of undoped GaN may be attributable to the dopants or

simply to differences in metal deposition methods in the construction of the diodes.

Regardless, the values of the effective Richardson constants differed considerably from

the theoretical value 26 A$\times$cm$^{-2}\times$K^{-2} [19, 24]. Hence, one should be cautioned when

using the theoretical value in traditional I-V measurements for determining the SBH as it

will likely be several orders of magnitude higher than the actual value.

V. Conclusions and Recommendations

5.1 Conclusions of Research

5.1.1 Schottky Barrier and Ideality

Overview

The Schottky barrier heights (SBH) calculated from the *I-V* and *I-V-T*

measurements (using the Jürgen Werner method [12] for *I-V* and modified Norde method

[8] for *I-V-T*) were in reasonable agreement with McHale's photoemission spectroscopy

results. Compared to his findings, the *I-V* measurements yielded SBH values of about

6% higher for the Gd-doped diode and 4% for the Er and Yb-doped diodes. For the *I-V-T*

measurements, the SBH was 11% lower for the Gd-doped diode and 15% lower for the

Er- and Yb-doped diodes. The statistical error generated from both methods overlapped,

which may compel one to speculate that the true SBH of the diodes lies somewhere

between the SBH determined from the two methods. This would be convenient

considering that McHale's results also fall within this same region of overlap in the

errors, but one should take caution with such a speculation because there is still a

statistical probability that the true SBH lies somewhere outside this region of overlap,

which cannot be ignored.

Non-Ideality of the Diodes

The cause of the high statistical errors in both measurements lies in the error

propagation in the extensive calculations required for non-ideal diodes, especially for the

I-V measurements needing the Jürgen Werner method [12]. This serves as a testament to

the importance of quality design and construction of the diodes. Recall that the ideality,

n, of the diodes were 5.972, 10.311 and 10.304 for Gd, Er and Yb respectively—significantly non-ideal. If the diodes showed an *n* somewhere between $n=1$ and $n=2$, then far more straight forward calculations could have been used to determine the SBH, thus reducing the statistical error.

The poor idealities are likely caused from faulty design and construction of the diodes. Evidence to support this lies in the large number of unusable diodes within the array of diodes applied to the thin films. Many diodes were measured and found to exhibit little to no rectification. During the hunt for a "good" diode, it became quickly evident that, for any given diode in the array, it was more likely to be useless than the opposite. Given the unusable quality of the majority of the diodes, it should come as no surprise that the "good" diodes were only labeled as such relative to the virtually useless diodes found before them. What, exactly, is to blame within the design and construction of the diodes is less likely to be a single point but rather a combination of factors.

Among the factors that may have degraded the quality of the diodes, many of them relate to affecting the interface specific region (ISR) in the metal-semiconductor junction. Recall that the ISR is critical in establishing the Schottky barrier and that irregularities in the ISR negatively impact the quality of the diode. Irregularities in the ISR lend themselves to an inhomogeneous Schottky barrier across the area of the junction. These irregularities can arise from a number of causes including contaminants in the metal or the semiconductor and poor post-deposition annealing. Not surprisingly, the quality of the surface of the semiconductor is also critical factor in forming a metal-semiconductor junction. Ultimately, the goal in metal deposition is to achieve a periodic

atomic structure in the ISR that "meshes", so to speak, with the periodic lattice of the semiconductor.

The surface quality of the GaN thin films was the greatest unknown quantity during the construction of the diode arrays. While considerable measures were taken to clean the surface of contaminants and oxides, little could be done to control for surface defects from physical damage that may have occurred do to careless handling or storage of the thin films. Ideally, the surface of the semiconductor would be a perfect cleave along a specified plane in the crystal lattice; achieving undisrupted periodicity in the atomic plane at the surface. Acknowledging that the thin films used in this study were the same thin films used in McHale's study, physical damage to the atomic periodicity at the surface of the semiconductor was probable considering the extensive handling and the storage methods. Additionally, there was no knowledge of the orientation of the crystal lattice of the semiconductor relative to the surface. In fact, as Tung points out, "surface states are not positioned inside the band gap of some semiconductor surfaces, such as the non-polar (110) surfaces of III-V semiconductors. So, on some cleaved non-polar surfaces, there is little band bending." [15]. Since GaN is a III-V semiconductor, there is always the possibility that the surface was the 110 plane of the GaN crystal lattice. If this was the case, then very little Schottky barrier would be observed, and in fact, the "good" diodes would be in regions where damage to the surface was greatest, contrary to intuition. In other words, it is possible, if the surface of the GaN was at the 110 plane, that the majority of the diodes in the array failed to sufficiently rectify because the surface of the semiconductor was unblemished and clean. Regardless, the point remains

that without knowledge of the crystal structure, condition and orientation of the

semiconductor, the quality of the metal contact depositions will always be suspect.

<u>Differences Between *I-V* and *I-V-T* Measurements</u>

The calculated SBHs of from the *I-V* data were universally higher than the

calculated SBHs from the *I-V-T* measurements. This may simply be a result of the

mathematical processes employed and the propagated statistical error in the calculations.

However, there may be another cause. Recall that the *I-V* measurements were performed

before the *I-V-T* measurements. It is possible that the currents in the diodes during the *I-

V* measurements damaged the diodes; causing a deteriorated SBH characteristic of the

diode.

The inhomogeneity of the SBH across the area of the contact results in a range of

differing parallel currents across the metal-semiconductor junction [15]. In the local

areas of the interface where the SBH is relatively low, the current density in that area will

be higher. One might argue that a high current density in a localized region of the

interface could alter the atomic structure of the ISR via Joule heating at that location and

exacerbate the inhomogeneity of the SBH; resulting in a degraded mean SBH across the

area of the interface. It is known that comparatively high currents were necessary under

reverse bias during the *I-V* measurements as the Jürgen Werner method required

exceeding the reverse voltage breakdown in the name of finding the parallel conductance,

G_P, of the diode. This was unavoidable in order to apply the Jürgen Werner method [12],

yet this very action may have produced enough current to alter the atomic structure of the

ISR. Additionally, when considering that the temperature of the sample was significantly

lowered after the *I-V* measurements were taken, there was little opportunity for the damage to "heal" itself in room temperature annealing. Thus, the order in which the measurements were taken, *I-V* measurements before *I-V-T* measurements, may have been an incorrect decision due to potential damage to the diode incurred during the *I-V* measurement.

It has also been considered that the cooling of the diodes may have contributed to the differences between the *I-V* results and the *I-V-T* results. Recall the high sensitivity to the nature of the probe contacts from Section 3.2.2. It may be possible that the ever so slight contraction of the stainless steel island or the contraction of the diode itself during cooling caused the nature of the probe contacts to change, resulting in a fundamental change in the nature of the circuit. While this seems unlikely, experience has taught that even the most seemingly insignificant alterations to the probe contacts will have a measurable effect on the *I-V* measurements.

5.1.2 Effective Richardson Constant

Also of note, was the effective Richardson constant, A^{**}. The Jürgen Werner method used in the *I-V* measurements required prior knowledge of A^{**}, which is often difficult to attain [8]. A value of $A^{**}=0.2$ A$\times$cm$^{-2}\times$K^{-2} was somewhat arbitrarily used as it seemed like a reasonable compromise between the theoretical value of 26 A$\times$cm$^{-2}\times$K^{-2} [19, 24] and experimentally determined values near of 0.001 A$\times$cm$^{-2}\times$K^{-2} [17, 18, 20, 24] for undoped GaN. This value was used in the SBH calculation from the *I-V* measurements of all three types of doped GaN. After the fact, it was observed that all of the calculated SBHs were universally higher than McHale's calculations, and that if the

value of A^{**} was changed to A^{**}=0.006 A×cm^{-2}×K^{-2} then the calculated SBH results of all three types of diode would be within no greater than 2% disagreement with McHale's results. Interestingly, the new value was in closer agreement to previous experimental work on undoped GaN [17, 18, 20, 24]. Owing that the theoretical value of A^{**}=26 A×cm^{-2}×K^{-2} was based on an ideal diode [19, 24] and that the diodes used in this work were far from ideal, the disagreement with theoretical values and agreement with experimental values should come as no surprise.

The speculated value of A^{**} was given some support by the calculated values determined by the Norde method [8] in the *I-V-T* method. The Norde method requires no prior knowledge of A^{**} and actually affords direct calculation of the value. All three calculated values of A** were higher than the speculated value, but they were still within the same range. A^{**} of the Gd-doped diode came closest to matching the speculated value (a difference of no more than 0.006 A×cm^{-2}×K^{-2}) followed by the Yb-doped diode and finally the Er-doped diode.

Ultimately, there was general consensus that the effective Richardson constants of rare earth doped GaN-based Schottky diodes should be somewhere just below 0.036 A×cm^{-2}×K^{-2}. This information may be useful to researchers in future work who are using the traditional method of determining the SBH in the traditional fashion on nearly ideal diodes via Equation (4) and Equation (5).

5.2 Significance of Research

In the name of SNM material detection, previous research has already determined that using a Gd-doped semiconductor diode detector is currently infeasible given

limitations in contemporary GaN growth capability, required electric potential in the detector, and noise limitations of common detector preamplifiers [7]. Thus, the known characteristics of Gd-doped GaN Schottky diodes can only serve as archival information with the hope that it may be referenceable when the other disciplines in crystal growth and preamplifier technologies improve sufficiently to support a working detector. However, in the field of semiconductor research, these results are of immediate interest.

The three measurement techniques used on the rare earth doped GaN thin films (photoemission spectroscopy done by McHale, and *I-V* measurements and *I-V-T* measurements done in this study) all indicate a measureable increase of about 25%-50% in the SBH over that of undoped GaN. This is of interest because an increased SBH corresponds to more efficient Schottky diodes due to reduced reverse current leakage. Additionally, in realm of LEDs, this work, in support of McHale's work, indicates that the photoemission potential of GaN-base LEDs might be effectively tuned by controlling dopant levels. In other words, the color of the light that we see emitted from the diode may be altered by simply controlling dopant levels in the GaN. For the semiconductor lighting industry, the results of this research warrant further investigation.

5.3 Recommendations for Future Research

The poor ideality of the diodes constructed in this research forced "exotic" mathematical treatment of the data (Jürgen Werner method [12] and modified Norde method [8]) in order to determine the SBH, which resulted in an undesirable propagation of error. However, *I-V-T* measurements, which suffered less error propagation than the *I-V* measurements, revealed that the effective Richardson constants of the three devices

were on par with pervious experimentally determined values on undoped GaN [17, 18, 20, 24]; far below the theoretical value [19, 24]. Using the calculated effective Richardson constants from this work, an effort to replicate this study using the traditional methods from Equation (4) and Equation (5) to determine the SBH may be justified on the condition that nearly ideal diodes, $n \simeq 1$, could be constructed. This method would yield results with less statistical error.

To build more ideal diodes, several recommendations are offered. Firstly, a complete knowledge of the doped GaN crystal lattice structure must be available before hand. Owing to the fact that the 110 plane of III-V semiconductors may result in substantially less band bending [15], the semiconductor should be cleaved such that this plane does not comprise the surface to which the metal contacts are deposited. The contact deposition method used in this study, electron beam vaporization epitaxy, is likely suitable. However, thermal annealing of the devices may reduce inhomogeneity of the SBH across the area of the contact and reduce the fragility of the ISR, thus it is recommended to add thermal annealing to the end of the metal contact deposition procedures. Thermal annealing has been used in previous research with success [20, 21, 23, 24] . Additionally, the size of the contacts should be reduced.

Taking into account the inhomogeneity of the SBH across the area of junction, it stands to reason that large contacts (i.e. large junction areas) are more vulnerable to a wider range in the SBH inhomogeneity. Previous research of this kind has used contacts of diameters on the order of a tenth of a millimeter with measureable success [17, 20, 21, 22, 23, 24, 26, 29]. The small contacts should afford less overall variation in the ISR. So as diodes in the array are measured, it can be assumed that they will either be nearly

completely functional or nearly completely useless with fewer diodes of quality in between.

Should these changes in the design and construction of the diodes be implemented, and it is found that the diodes still do not meet the ideality criteria, $n \simeq 1$, then a modified measurement method is proposed. Firstly, the *I-V-T* measurements should be performed prior to the *I-V* measurements for the reasons outlined in Section 5.1.1. Secondly, the *I-V* measurements should follow merely for the purpose of determining the value of n. A hybrid of the Jürgen Werner method [12] and the modified Norde method [8] could be used. Only the first few steps in the Jürgen Werner method would be used in order to determine the exact value of n. The value of n could then be passed to the modified Norde method, which would be used in its entirety to determine the SBH and the effective Richardson constant.

In summary, results with less statistical error may be available in replication of this work if the researcher can improve upon the ideality of the diodes by having prior knowledge of the semiconductor crystal lattice orientation, reducing the size of the contacts and thermally annealing the diodes post-construction. The researcher could then use the traditional method of finding the SBH by using the values of A^{**} (determined in this work) with Equation (4) and Equation (5), or as an alternative, should the diodes still be less than ideal, use the hybridized version of the Jürgen Werner / Norde methods.

5.4 Summary

This research involved depositing Schottky contacts on the surfaces of rare earth doped GaN thin films in order to find the Schottky barrier heights of the materials via *I-V*

measurements and *I-V-T* measurements. The results of these measurements were compared to the results of photoemission spectroscopy measurements previously performed by McHale [15]. All three measurements were in agreement with regards to showing that Yb-doped GaN had the highest Schottky barrier height and Gd had the lowest, but conclusive statements about the exact values cannot be made due to the high statistical error in the results in this stud . The statistical error arose as error propagation through the calculations that were necessary to deal with non-ideal Schottky diodes. The poor ideality of the diodes required using the Jürgen Werner method [12] to analyze the *I-V* data, which resulted in the highest errors. The modified Norde method [8] was used to analyze the *I-V-T* data and produced less error, but the determined barrier heights were universally lower than those determined by the *I-V* Jürgen Werner method. It should be noted that the act of performing the *I-V* measurements may have slightly degraded the SBH before the *I-V-T* measurements were taken. Ultimately, the results are interesting with respect to the fact that the error of both types of measurement overlapped, and that McHale's photoemission spectroscopy measurements fell between the high *I-V* calculated Schottky barrier heights and the low *I-V-T* calculated heights. There is now evidence from three different measurement techniques to support the idea that rare earth doping of GaN semiconductors will increase the Schottky barrier height by at least 20%.

Bibliography

[1] United States Nuclear Regulatory Commission (NRC).
   http://www.nrc.gov/materials/sp-nucmaterials.html Accessed 13 Dec 2012

[2] Knoll, Glenn. *Radiation Detection and Measurement*. New Jersey: John Wiley &
   Sons, 2010.

[3] Krane, Kenneth. *Introductory Nuclear Physics*. New Jersey: John Wiley & Sons,
   1988.

[4] Lederer, C., Shirley, V. *Table of Isotopes (7ᵗʰ Ed)*. New York: John Wiley & Sons,
   1978.

[5] Bridgman, Charles J. *Introduction to the Physics of Nuclear Weapons Effects*. Fort
   Belvoir, VA: Defense Threat Reduction Agency, 2001.

[6] Seymour, R.; Crawford, T.; et. al. (2001). Portal, freight and vehicle monitor
   performance using scintillating glass fiber detectors for the detection of plutonium in
   the Illicit Trafficking Radiation Assessment Program. *Journal of Radioanalytical and
   Nuclear Chemistry, 248,* 699–705.

[7] McHale, Stephen R. "The Effects of Rare Earth Doping On Gallium Nitride Thin
   Films," AFIT Dissertation AFIT/DS/ENP/11-S05, (Sep 11)

[8] Schroder, Dieter. *Semiconductor Material and Device Characterization*. New York:
   John Wiley & Sons, 1990.

[9] McKelvey, John P. *Solid State Physics for Engineering and Materials Science.*
   Florida: Krieger Publishing Co, 1993.

[10] Sze, Simon M. *Physics of Semiconductor Devices*. New Jersey: John Wiley and
   Sons, 2007.

[11] Sze, S. *Semiconductor Devices, Physics and Technology*. New Jersey: John Wiley
   & Sons, 1985.

[12] Werner, J.H. (1988). Schottky barrier and pn-junction I/V plots—small signal
   evaluation. *Applied Physics A (Solids and Surfaces) 47*, 291-300.

[13] Klein, C.A. (1968). Bandgap dependence and related features of radiation ionization
   energies in semiconductors. *Journal of Applied Physics*, *39*(4), 2029–2038.

[14] US Department of Energy, *Solid State Lighting*,
http://www1.eere.energy.gov/buildings/ssl/ . Accessed 6 Jan 2013.

[15] Tung, Raymond T. *Brooklyn College Schottky Barrier Height Tutorial
(Inhomogeneous Schottky Barriers)*, Web version.
http://academic.brooklyn.cuny.edu/physics/tung/Schottky/inhomo.htm Accessed 6
Jan 2013

[16] Eisberg, R., Resnick, R. *Quantum Physics of Atoms, Molecules, Solids, Nuclei, and
Particles.* Toronto: John Wiley & Sons, 1974.

[17] Binari, S.C. *et. al* (1994). Electrical characterization of Ti Schottky barriers on *n*-
type GaN. *Electronics Letters, 30*(11), 909-910.

[18] Guo, J.D. *et. al* (1996). Schottky contact and the thermal stability of Ni on *n*-type
GaN. *Journal of Applied Physics, 80*(3), 1623-1627.

[19] Doğan, S., Duman, S., Gürbulak, B., Tüzemen, S., Morkoc, H. (2009). Temperature
vriation of current-voltage characteristics of Au/Ni/n-GaN Schottky diodes. *Physica
E., 41*, 646-651.

[20] Hacke, P., Detchprohm, T., Kiramatsu, K., Sawaki, N. (1993). Schottky barrier on
n-type GaN grown by hydride vapor phase epitaxy. *Applied Physics Letters, 63*(19),
2676-2678.

[21] Kribes, Y., Harrison, I., Tuck, B., Cheng, T.S., Foxon, C.T. (1997). Investigation of
Au Schottky contacts on GaN grown by molecular beam epitaxy. *Semiconductor
Science and Technology, 12,* 913-916.

[22] Miller, E.J. *et. al* (2003). Reverse-bias leakage current reduction in GaN Schottky
diodes by electrochemical surface treatment. *Applied Physics Letters, 82*(8), 1293-
1295.

[23] Miller, E.J., Yu, E.T., Walterseit, P., Speck, J.S. (2004). Analysis of reverse-bias
leakage current mechanisms in GaN grown by molecular-beam epitaxy. *Applied
Physics Letters, 84*(4), 535-537.

[24] Khan, M.R.H., Detchprohm, T., Hacke, P., Hiramatsu, K., Sawaki, N. (1995). The
barrier height and interface effect of a Au—n-GaN Schottky diode. *Journal of
Physics D: Applied Physics, 28,* 1169-1174.

[25] Ping, A.T., Schmitz, A.C., Asif Khan, M., Adesida, I. (1996). Characterisation of Pd Schottky barrier on *n*-type GaN. *Electronics Letters, 32*(1), 68-70.

[26] Schmitz, A.C. *et. al* (1996). Schottky barrier properties of various metals on *n*-type GaN (letter to the editor). *Semiconductor Science Technology, 11,* 1464-1467.

[27] Wang, X.J., He, L. (1998). Electrical characteristics of high performance Au/*n*-GaN Schottky diodes. *Journal of Electronic Materials, 27*(11), 1272-1276.

[28] Cibils, R.M., Buitrago, R.H. (1985). Forward *I-V* plot for nonideal Schottky diodes with high series resistance. *Journal of Applied Physics 58,*(2), 1075-1077.

[29] Wang, K., Wang, R.X. (2005). Film thickness degradation of Au/GaN Schottky contact characteristics. *Materials Science and Engineering B, 117,* 21-25.

[30] Wikipedia. *Lightning.* http://en.wikipedia.org/wiki/Lightning . Accessed 6 Jan 2013.

[31] Aubry V., Meyer F. (1994). Schottky diodes with high series resistance: Limitations of forward I-V methods. *Journal of Applied Physics 76*(12), 7973-7984.

[32] Lien, C.D., So, F.C.T., Nicolet, M.A. (1984). An improved forward IV method for non-ideal Schottky diodes with high series resistance. *Electron Devices 31*(10), 1502-1503.

REPORT DOCUMENTATION PAGE

1. REPORT DATE *(DD-MM-YYYY)*	2. REPORT TYPE	3. DATES COVERED *(From – To)*
21 Mar 2013	Master's Thesis	04 Sep 2011 - Mar 2013

4. TITLE AND SUBTITLE

ELECTRONIC CHARACTERISTICS OF RARE EARTH DOPED GaN SCHOTTKY DIODES

5a. CONTRACT NUMBER

5b. GRANT NUMBER

5c. PROGRAM ELEMENT NUMBER

6. AUTHOR(S)

Blanning, Aaron B., Major, USA

5d. PROJECT NUMBER
N/A

5e. TASK NUMBER

5f. WORK UNIT NUMBER

7. PERFORMING ORGANIZATION NAMES(S) AND ADDRESS(S)

Air Force Institute of Technology
Graduate School of Engineering and Management (AFIT/ENV)
2950 Hobson Way, Building 640
WPAFB OH 45433-8865

8. PERFORMING ORGANIZATION REPORT NUMBER

AFIT-ENP-13-M-03

9. SPONSORING/MONITORING AGENCY NAME(S) AND ADDRESS(ES)

DEFENSE THREAT REDUCTION AGENCY   (Col Jeffrey Musk)
8725 JOHN J KINGMAN RD STOP 6201
FORT BELVOIR VA 22060-6201
(703) 767-5870, (DSN 427) dtra.publicaffairs@dtra.mil

10. SPONSOR/MONITOR'S ACRONYM(S)
DTRA OP/CSU

11. SPONSOR/MONITOR'S REPORT NUMBER(S)

12. DISTRIBUTION/AVAILABILITY STATEMENT
APPROVED FOR PUBLIC RELEASE; DISTRIBUTION UNLIMITED

13. SUPPLEMENTARY NOTES

14. ABSTRACT
The Schottky barrier height (SBH) was measured on GaN based diodes with three different dopant types; Gd, Er and Yb. Two methods were used to determine the SBH. The first method was the Jürgen Werner method to evaluate the *I-V* characteristics. The calculated SBH of the diodes using this method was 1.41 ± 0.20eV, 1.71 ± 0.25eV and 1.75 ± 0.28eV for the Gd-, Er- and Yb-doped diodes respectively. It was observed that using an ad-hoc effective Richardson constant value of $0.006 A\times cm^{-2}\times K^{-2}$ to calculate the SBH rendered results that were in no greater than 2% disagreement (neglecting error) with photoemission spectroscopy measurements performed on the same GaN thin films by a another researcher a year prior. The second method of measuring the SBH was the temperature dependent *I-V-T* measurements using the modified Norde function. The calculated SBH of the diodes are universally lower than the results of the Jürgen Werner method. The SBH was 1.19 ± 0.12eV, 1.39 ± 0.16eV and 1.43 ± 0.12eV for the Gd-, Er- and Yb-doped diodes respectively. Additionally, the Norde method provided direct calculation of the effective Richardson constants, which were $0.011\pm0.001 A\times cm^{-2}\times K^{-2}$, $0.036\pm0.003 A\times cm^{-2}\times K^{-2}$ and $0.021\pm0.02 A\times cm^{-2}\times K^{-2}$ for the Gd-, Er- and Yb-doped diodes respectively. Both measurements in this study are in agreement with the earlier photoemission spectroscopy measurements with regard to the proportional differences among the different dopant types.

15. SUBJECT TERMS

Rare earth doping, Gallium Nitride, Thin films, Schottky barrier, Schottky diode, Neutron detection

16. SECURITY CLASSIFICATION OF:			17. LIMITATION OF ABSTRACT	18. NUMBER OF PAGES	19a. NAME OF RESPONSIBLE PERSON
a. REPORT	**b. ABSTRACT**	**c. THIS PAGE**			LTC Stephen R. McHale AFIT/ENP
U	U	U	UU	114	**19b. TELEPHONE NUMBER** *(Include area code)* 937-255-3633 x4438; stephen.mchale@afit.edu